# Sorting of secretory proteins at the trans-Golgi network by TGN46

Pablo Lujan[1], Carla Garcia-Cabau[2,#], Yuichi Wakana[3,#], Carmen Rodilla-Ramírez[1], Vivek Malhotra[4,5,6], Xavier Salvatella[2,6], Maria F. Garcia-Parajo[1,6], and Felix Campelo[1,*]

[1] ICFO-Institut de Ciencies Fotoniques, The Barcelona Institute of Science and Technology, 08860, Castelldefels (Barcelona), Spain.

[2] Institute for Research in Biomedicine (IRB Barcelona), The Barcelona Institute of Science and Technology, Baldiri Reixac 10, 08028, Barcelona, Spain.

[3] School of Life Sciences, Tokyo University of Pharmacy and Life Sciences, Hachioji, Tokyo 192-0392, Japan.

[4] Centre for Genomic Regulation (CRG), The Barcelona Institute of Science and Technology, Barcelona, Spain.

[5] Universitat Pompeu Fabra (UPF), Barcelona, Spain.

[6] Institució Catalana de Recerca i Estudis Avançats (ICREA), Passeig Lluís Companys 23, 08010, Barcelona, Spain.

[#] These authors contributed equally

[*] **Correspondence:**

Felix Campelo

ICFO-Institut de Ciencies Fotòniques

Av. Carl Friedrich Gauss, 3. 08860 Castelldefels, Barcelona - SPAIN

Phone: + 34 93 554 2225

e-mail: felix.campelo@icfo.eu

## ABSTRACT

Secretory proteins are sorted at the trans-Golgi network (TGN) for export into specific transport carriers. However, the molecular players involved in this fundamental process remain largely elusive. Here, we identified the transmembrane protein TGN46 as a cargo receptor for the export of secretory proteins in CARTS – a class of protein kinase D-dependent TGN-to-plasma membrane carriers. We show that TGN46 is necessary for cargo sorting and loading into nascent carriers at the TGN. By combining quantitative fluorescence microscopy and mutagenesis approaches, we further discovered that the TGN46 lumenal domain encodes for its cargo sorting function. Interestingly, this domain forms liquid droplets in vitro by means of liquid-liquid phase separation, a physical mechanism that may assist in TGN46-mediated cargo sorting. In summary, our results define a cellular function of TGN46 in sorting secretory proteins for export from the TGN. These findings could open new therapeutic avenues for diseases that parallel secretory malfunction.

**KEYWORDS:** Golgi apparatus, transport carrier, liquid-liquid phase separation, protein kinase D, export kinetics, membrane trafficking.

## INTRODUCTION

Biosynthetic secretory cargoes are made in the ER and transported to the Golgi apparatus, where they are further processed and eventually sorted at the *trans*-Golgi network (TGN) for delivery to their respective destinations [1–5]. The accurate and timely export of cargo proteins is essential for the maintenance of cell and tissue homeostasis, and, accordingly, errors in this process can have severe physiological and pathophysiological consequences [6]. Despite the importance of this process, identification of the molecular machinery and the mechanisms of cargo sorting at the TGN remain largely elusive [7–10]. In mammalian cells, lysosomal hydrolases bearing a mannose 6-phosphate are sorted by the mannose 6-phosphate receptors into clathrin-coated vesicles for their transport to the endo-lysosomal system [11,12]. By contrast, no coats have been identified for most export routes from the TGN – especially for those destined to the cell surface [1,2] –, which has hampered the identification of cargo receptors and/or of other sorting modules. The discovery by Malhotra and colleagues of a $Ca^{2+}$-dependent mechanism for the sorting of soluble secretory cargoes is beginning to reveal the intricacies of this supposedly receptor-independent process [13,14]. This mechanism relies on the coordinated action of a subset of cellular components, including the actin filament-severing protein cofilin [13,14], the $Ca^{2+}$ pump SPCA1 [15,16], the oligomeric lumenal $Ca^{2+}$-binding protein Cab45 [17,18], and the sphingolipid sphingomyelin (SM) [19,20]. The export from the Golgi by this pathway is independent of COPI or clathrin coats and no other coat proteins have been identified thus far. The single-pass type I transmembrane (TM) protein TGN46 – or TGN38 in the mouse system [21] – has been proposed to be a secretory cargo receptor [10,22–27]. However, a direct demonstration of TGN46 in export of secretory cargoes is lacking.

TGN38 was first identified in rat cells and shown to have a well-defined steady-state localization at the TGN membrane [28], making TGN38 and its orthologues be widely used as TGN marker proteins. Remarkably, the amino acid sequence of rat TGN38 is largely conserved amongst other species, including humans (>80% amino acid identity between rat TGN38 and human TGN46), with highly-conserved cytosolic and TM domains and a somewhat less conserved lumenal domain (>60% overall identity but only ~25% in the bulk of the lumenal domain) [21]. Despite its steady-state TGN localization, TGN38 cycles between the TGN and the plasma membrane via endosomes [25,29–32]. TGN46 exits the TGN in specific carriers called CARTS (carriers of the TGN to the cell surface). Protein kinase D (PKD), known for its role in events leading to the fission of cargo-containing carriers at the TGN, is required for the production of CARTS [2,33–35]. How secretory cargoes are sorted and specifically packed into CARTS is not known. Interestingly, TGN46 has been recently reported to assist in the trafficking of severe acute respiratory syndrome coronavirus 2 (SARS-CoV-2), as this protein is upregulated in SARS-CoV-2-infected cells and cells depleted of TGN46 showed a reduced

SARS-CoV-2 infection rate [36]. Understanding the mechanisms of TGN46-assisted membrane trafficking will therefore be of upmost importance to assist in the rational design of new therapeutic tools to target human pathologies associated with defects in the secretory pathway.

Here we demonstrate that TGN46 plays a key role in the export of secretory cargoes, specifically in the sorting of the CARTS-specific soluble cargo protein pancreatic adenocarcinoma upregulated factor (PAUF). Our data reveal that the topological determinants that describe the proper intracellular and intra-Golgi localization of TGN46, as well as its own incorporation in CARTS, are mainly contained in its lumenal domain. Notably, we find that the lumenal domain of TGN46 is both necessary and sufficient for the export of cargo proteins into CARTS and, moreover, that this domain mediates the cargo sorting function of TGN46. We show that, *in vitro*, the lumenal domain of TGN46 forms liquid droplets by a liquid-liquid phase separation (LLPS) mechanism. Altogether, our data suggest an essential role for TGN46 in the sorting of cargo proteins into transport carriers (CARTS) at the TGN. Based on our *in vitro* data, we propose that LLPS in the lumen of the TGN may assist in cargo sorting by TGN46 into CARTS.

## RESULTS

### TGN46 is required for cargo sorting into CARTS

As TGN46 has been suggested to be involved in cargo sorting at the TGN, we decided to test this hypothesis. We generated a TGN46-lacking line of Hela cells by CRISPR/Cas9-mediated knock out of *TGOLN2* – the gene encoding for human TGN46 (TGN46-KO cell line) (***Fig. 1A*** and ***Fig. S1A***). To test if TGN46 is required for CARTS-mediated secretion, we transiently expressed a CARTS-specific soluble cargo protein, PAUF-MycHis, in both parental and TGN46-KO cells. Both the medium and cell lysates were collected and analyzed by western blotting with an anti-Myc antibody to detect the secreted and internal PAUF-MycHis pools, respectively. In TGN46-KO cells, PAUF-MycHis secretion was reduced to ~25% of the levels observed in control cells (***Fig. 1A***). Surprisingly, we noted a lower molecular weight form of PAUF-MycHis in the lysate of TGN46-KO cells (***Fig. 1A***), implying that the processing (e.g., glycosylation) of intracellularly accumulated PAUF-MycHis is incomplete, and suggesting a potential role for TGN46 in facilitating cargo glycosylation. Immunofluorescence microscopy of cells expressing PAUF-mRFP revealed its presence in a perinuclear compartment and punctate cytoplasmic vesicular structures in both cell lines, indicating that PAUF-mRFP efficiently exits the ER and accumulates in the Golgi apparatus in the absence of TGN46 (***Fig. S1A***).

To test whether TGN46 is specifically involved in the secretion of CARTS-mediated cargoes or rather plays a general role in TGN export, we simultaneously monitored Golgi export of PAUF-mRFP (a CARTS cargo) and VSVG-HA (a non-CARTS cargo) [2,33] in control and TGN46-KO cells. We used the standard temperature-induced block in cargo export at the TGN to monitor synchronous exit of VSV-G and PAUF in control and TGN46-lacking cells. Cells were first incubated at 20ºC for 2h to block TGN export, and subsequently shifted to 37ºC for 15 min to allow for synchronized cargo export from the TGN, after which cells were fixed and the number of cargo-containing vesicular structures per unit area was analyzed by confocal fluorescence microscopy (***Fig. 1B*** and ***Fig. S1B***). Our results show that the number of PAUF-mRFP-positive punctate structures – mostly corresponding to CARTS [33] – is significantly reduced in TGN46-KO cells as compared to control cells (***Fig. 1B***), which agrees with the observed inhibition of PAUF secretion in the absence of TGN46 (***Fig. 1A***). In contrast, the density of VSVG-containing carriers was unaltered upon TGN46 depletion (***Fig. 1B*** and ***Fig. S1B***), suggesting a CARTS-specific role of TGN46 in cargo export at the TGN. In addition, TGN46 depletion did not increase the percentage of PAUF-mRFP-containing carriers that also contain VSVG-HA (***Fig. S1C***). These data strongly suggest that, in the absence of TGN46, PAUF is not re-routed towards alternative TGN export routes (particfularly to that of VSV-G-containing transport carriers), and therefore bona fide CARTS are still formed, although at a reduced rate.

We next assessed by fluorescence loss in photobleaching (FLIP) microscopy the residence time of PAUF in the Golgi apparatus, which is a dynamic measure of the Golgi export rate of this cargo (***Fig. S1D***) [37,38]. In our FLIP experiments, we systematically photobleached the entire pool of fluorescent protein (PAUF-mRFP) outside of the perinuclear Golgi area by using a high intensity laser, and measured the decay of the fluorescence intensity of the Golgi area as function of time (***Fig. S1D***). Thus, for cargo proteins that are rapidly exported from the Golgi, the fluorescence intensity in the Golgi area rapidly decays, whereas for resident Golgi proteins, the fluorescence decays more slowly. Our results showed that PAUF-mRFP has a longer Golgi residence time in TGN46-KO cells (~40 min) as compared to control cells (~25 min), and therefore TGN46 is necessary for an efficient and fast export of PAUF (***Fig. 1C,D*** and ***Fig. S1D***). Taken together, our results indicate that TGN46 is necessary for CARTS-mediated PAUF export from the TGN.

**TGN46 is required for cargo loading into CARTS**

The kinase activity of protein kinase D (PKD) is required for severing CARTS from the TGN [33]. Expression of a kinase-dead mutant of PKD (PKD-KD) induces formation of cargo-containing tubules (fission-defective CARTS precursors) at the TGN [2,39]. We took advantage

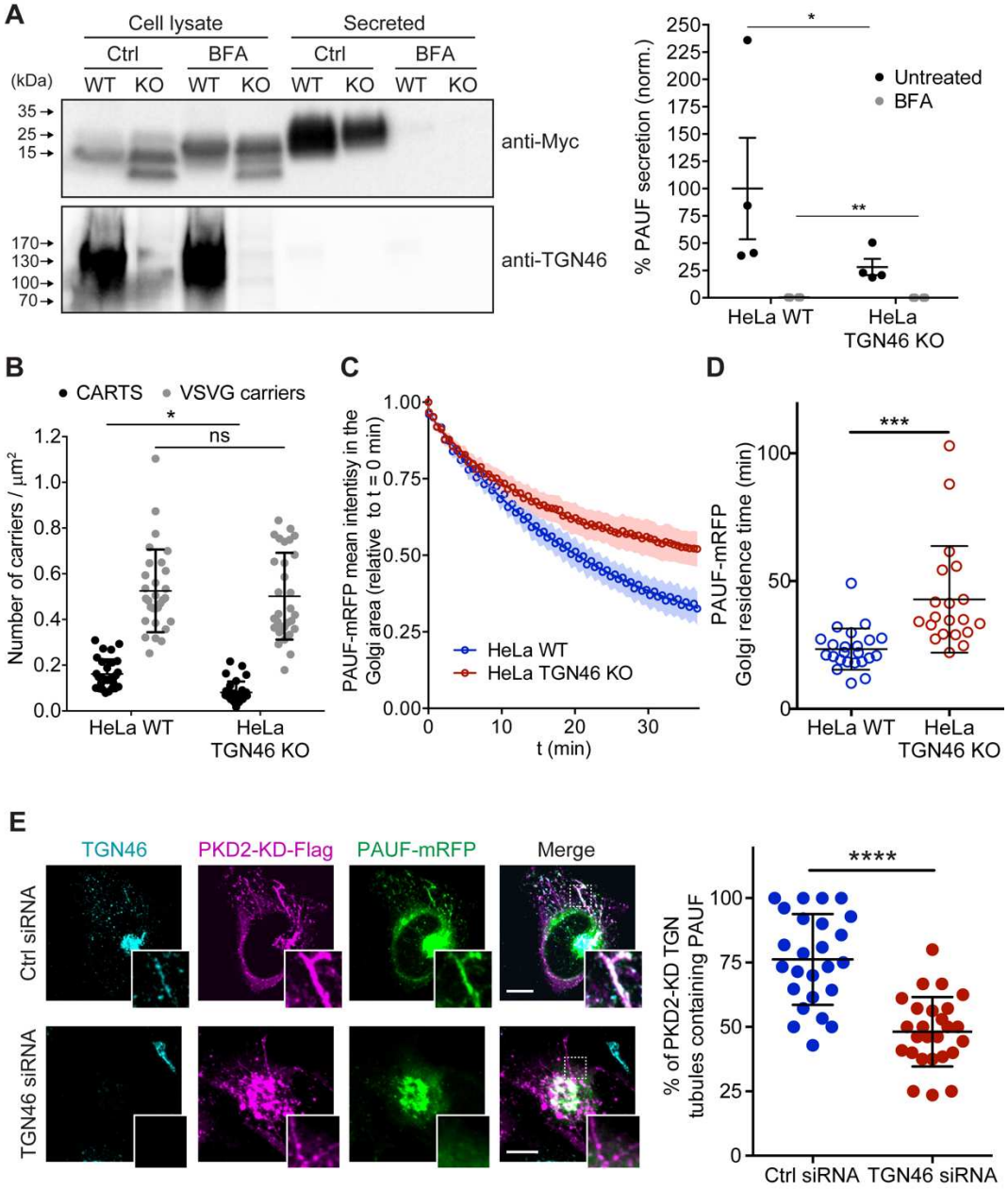


**Figure 1. TGN46 is required for cargo sorting and loading into CARTS. (A)** PAUF secretion assay in parental (WT) and CRISPR/Cas9-mediated TGN46 knockout (KO) HeLa cells. Cells expressing PAUF-MycHis were incubated for 4 h in fresh medium without serum in the absence (Ctrl) or presence of Brefeldin A (BFA), after which the cells were lysed. Equal amounts of cell lysates and their corresponding secreted fraction (medium) were analyzed by western blotting (left) using an anti-Myc antibody (top blot) and anti-TGN46 antibody (bottom blot). BFA was included as a positive control of secretion inhibition. Quantification (right) of the ratio of secreted/internal PAUF signal normalized (norm.) as a percentage to the average value of the WT, Ctrl condition. n=4 independent experiments. Individual values shown, with mean ± stdev. **(B)** Number of carriers (CARTS, black symbols; VSVG carriers, gray symbols) per unit area observed in WT or TGN46 KO HeLa cells expressing either PAUF-mRFP (CARTS marker) and VSVG-HA (VSVG carrier marker). At least 10 cells from each of n=3 independent experiments were quantified. Individual values shown, with mean ± stdev. **(C)** Relative fluorescence intensity average time trace (mean ± s.e.m.) of FLIP experiments performed in WT or TGN46 KO HeLa cells expressing PAUF-mRFP. **(D)** Quantification of the PAUF-mRFP Golgi residence time as obtained from the FLIP experiments, as the one shown in **(C)**. Between 7–12 cells from each of n=3 independent experiments were quantified. Individual values shown, with mean ± stdev. **(E)** Left panels are confocal fluorescence microscopy images of HeLa cells transfected with control (Ctrl) or TGN46 siRNA, which were also transfected with PKD2-KD-Flag and PAUF-mRFP. Cells were fixed at steady state and labelled with anti-TGN46 (cyan) and anti-Flag (magenta) antibodies. PAUF-mRFP fluorescence signal is shown in green. Scale bars are 10 µm, magnifications of the boxed regions are shown. In the right panel, the quantification of the percentage of PKD2-KD-induced tubules that containg PAUF-mRFP in control (Ctrl) or TGN46 siRNA-treated cells. At least 10 cells from each of n=3 independent experiments. Individual values shown, with mean ± stdev.

of this finding to investigate the role of TGN46 in PAUF export in CARTS. We silenced TGN46 expression in HeLa cells by siRNA, and co-transfected PAUF-mRFP and PKD2-KD-Flag in control and TGN46-depleted cells, after which cells were fixed and processed for immunofluorescence microscopy. TGN46 depletion did not affect the number of PKD2-KD-positive TGN tubules per cell (***Fig. 1E*** and ***Fig. S1E***). As previously reported, the Golgi tubules observed in control cells contained both TGN46 and PAUF-mRFP (***Fig. 1E***) [33,40]. In contrast, and remarkably, PAUF-mRFP was absent in most PKD-KD-induced tubes observed in TGN46-depleted cells (~45±10%) compared to tubules in control cells (~75±15%) (***Fig. 1E*** and ***Fig. S1E***). These findings strongly support the requirement of TGN46 in the sorting and/or packaging of the model cargo protein PAUF into nascent CARTS at the TGN.

**TGN46 export in CARTS is not dependent on cytosolic tail signals**

Although a number of sequence motifs have been reported to serve as retention signals for Golgi-resident proteins [41,42], less is known about how cargoes are selectively sorted into transport carriers budding at the TGN. Particularly, no sorting mechanism has been reported for CARTS-specific cargoes [2]. To gain insight into how TGN46 drives selective cargo incorporation into nascent transport carriers, we asked whether TGN46 contains dedicated topological determinants (such as domains, regions, or motifs) for its cargo sorting/packaging function. As TGN46 is a single-pass, type I TM protein of 437 amino acids (human TGN46, UniProt identifier O43493-2), we investigated whether functional cargo-packaging modules can be found in *(i)* the N-terminal lumenal domain (amino acids 22–381), *(ii)* the single TM domain (TMD; amino acids 382–402), and/or *(iii)* the short C-terminal cytosolic tail (amino acids 403–437). In particular, we evaluated how each of these domains contributes to TGN46 function in loading cargoes into CARTS by investigating their role in *(i)* protein localization to TGN export domains, *(ii)* specific incorporation into CARTS, and *(iii)* defining the Golgi export rate of the cargo proteins.

The cytosolic tail of TGN46 contains a tyrosine-based cytosolic motif (YXXΦ; where X represents any amino acid, and Φ is an amino acid with bulky hydrophobic side chains [43]; in TGN46: YQRL, amino acids 430-433), which is crucial for the localization of TGN46 at TGN, because it acts as an endocytic signal for plasma membrane internalization and trafficking back to the TGN [22,25,29,30,32,44]. We expressed in HeLa cells a GFP-tagged deletion mutant of TGN46 lacking the cytosolic domain but maintaining the lumenal domain and TMD (GFP-TGN46 LT) (***Fig. 2A***) and analyzed its intracellular localization by fluorescence microscopy. GFP-TGN46 LT was mostly present at the *trans*-Golgi membranes/TGN, as qualitatively seen in the micrographs (***Fig. S2A***). To quantitatively measure whether the intra-Golgi localization of this protein is similar or not to that of wild type TGN46 (TGN46 WT), we then measured the degree

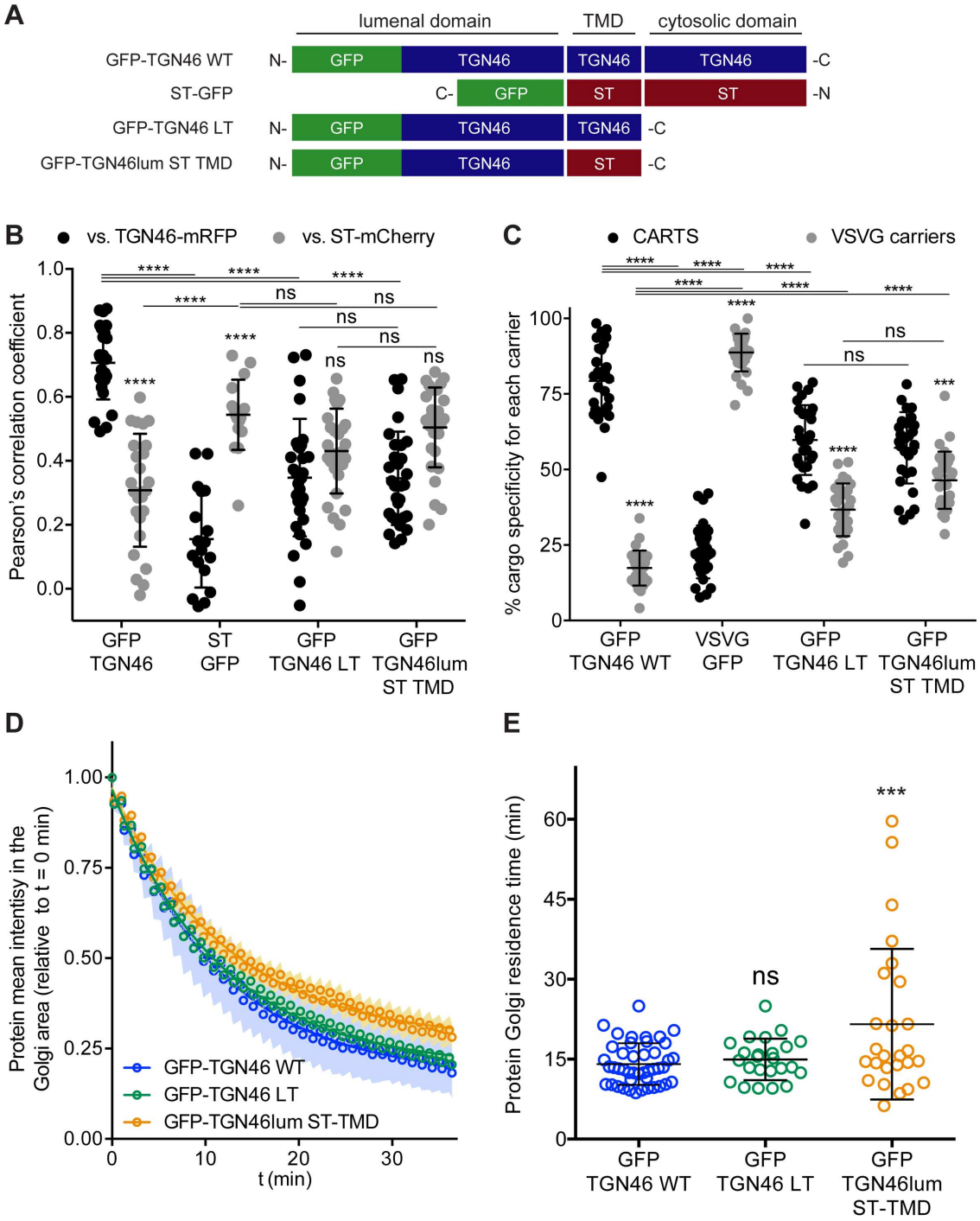


**Figure 2. TGN46 export in CARTS is not dependent on cytosolic tail signals. (A)** Schematic representation of construct domain topology. Notice that type I proteins (e.g., GFP-TGN46-WT) have a lumenal N-terminal domain, whereas type II proteins (e.g., ST-GFP) have a cytosolic N-terminal domain. TMD: transmembrane domain. **(B)** Pearson's correlation coefficient between the perinuclear fluorescence signal of the x-axis indicated proteins with respect to TGN46-mRFP (black symbols) or ST-mCherry (gray symbols), measured from confocal micrographs of HeLa cells expressing the indicated proteins. Results are from at least 10 cells from each of n=3 independent experiments (individual values shown, with mean ± stdev). **(C)** Percentage of transport carriers containing each of the cargoes described on the x-axis that are also positive for PAUF (CARTS, black symbols) or VSVG (VSVG carriers, gray symbols), as measured from confocal micrographs of HeLa cells expressing the indicated proteins. Results are from at least 10 cells from each of n=3 independent experiments (individual values shown, with mean ± stdev). **(D)** Relative fluorescence intensity average time trace (mean ± s.e.m.) of FLIP experiments for the indicated proteins. Symbols correspond to actual measurements, solid lines to the fitted exponential decays. **(E)** Residence time in the perinuclear area measured as the half time of the FLIP curves. Results are from 7–12 cells from each of n=3 independent experiments (individual values shown, with mean ± stdev).

of perinuclear colocalization (Pearson's correlation coefficient; [45]) of either GFP-TGN46 WT or GFP-TGN46 LT with respect to TGN46-mRFP and the *trans*-Golgi-resident glycosylation enzyme sialyltransferase (ST) tagged with mCherry (ST-mCherry) (***Fig. 2B*** and ***Fig. S2A***). Our data show that GFP-TGN46 LT has a lower degree of intra-Golgi colocalization with respect to TGN46-mRFP and a higher one with respect to ST-mCherry, as compared to its WT counterpart (***Fig. 2B*** and ***Fig. S2A***). Hence, GFP-TGN46 LT shows an intra-Golgi localization pattern more closely resembling that of ST-GFP (***Fig. 2B*** and ***Fig. S2A***). These data indicate that the cytosolic domain of TGN46 not only confers an overall TGN localization as previously reported [29,32], but it also contributes to its steady-state localization in TGN export domains (TGN46 WT-positive regions, which also include the TGN regions involved in TGN46 recycling from the endosomes) as compared to processing domains (ST-positive regions). We therefore hypothesized that the cytosolic tail-lacking TGN46 mutant could also have a compromised export from the TGN. To test this, we first monitored the incorporation of GFP-TGN46 LT into CARTS. HeLa cells co-overexpressing GFP-TGN46 LT together with either PAUF-mRFP (CARTS marker) or VSVG-HA (a CARTS-independent TM cargo protein) were incubated at 20ºC for 2 h to inhibit TGN export, shifted to 37ºC for 15 min to re-initiate cargo export, fixed, and imaged by fluorescence microscopy. We then analyzed the fraction of cargo-containing carriers (for three different cargoes: GFP-TGN46 WT, VSVG-HA, and GFP-TGN46 LT) that were also positive for PAUF-mRFP (CARTS) or VSVG-HA (VSVG carriers). Our results indicated that GFP-TGN46 LT is preferentially exported in CARTS and not in VSVG carriers, although this mutant cargo protein showed a slight but significant decrease in its CARTS specificity as compared to GFP-TGN46 WT (***Fig. 2C*** and ***Fig. S2B***). We next performed FLIP experiments to measure the Golgi residence time of GFP-TGN46 LT, and compare it with that of GFP-TGN46 WT. Interestingly, the deletion mutant GFP-TGN46 LT exited the Golgi apparatus at a rate that was indistinguishable from that of GFP-TGN46 WT (***Fig. 2D,E*** and ***Fig. S2C***). Taken together, our results suggest that *(i)* the TGN46 cytosolic tail appears to play a minor role in driving steady state localization to TGN export domains as well as in CARTS selectivity; and *(ii)* the mutant of TGN46 lacking the cytosolic tail still remains a bona fide CARTS cargo that is exported at a normal rate.

**TGN46 intra-Golgi localization and CARTS specificity are insensitive to TMD length and composition**

We next investigated if the information encoded in the amino acid sequence of the TGN46 TMD determines its incorporation into CARTS. The hydrophobic matching hypothesis is a TMD-based sorting mechanism that has been proposed to contribute to the retention of Golgi-resident TM proteins [41,42]. This mechanism is based on the hypothesis that single-pass TM proteins preferably partition into membranes with a thickness that matches the hydrophobic

length of the protein TMD [46–48]. The membrane thickness increases along the secretory pathway [49], which correlates with the average length of the TMDs of differentially-localized proteins along the secretory pathway [47]. Hence, according to the TMD-based retention hypothesis, the segregation between Golgi-resident proteins and cargoes en route to be exported from the TGN would be based on the different physical properties of the lipids and proteins composing such domains [47,48,50,51]. TGN46 is a type I protein with a single TMD of 21 amino acids, whereas ST (ST6Gal-I) – a Golgi-resident type II protein that also localizes to *trans*-Golgi membranes – has a shorter TMD of 17 amino acids (***Fig. 3A***). Thus, to test whether the length of the TMD of TGN46 is important for its intra-Golgi localization, selective CARTS-mediated export, and Golgi residence time, we generated two different TGN46 mutants by altering its TMD sequence: a TGN46 ΔAAIL mutant that lacks 4 amino acids (AAIL) in the central region of the TMD; and a TGN46-ST TMD mutant, in which we replaced the TGN46 TMD by that of ST, while keeping the orientation and, therefore, the correct topology of the TMD (***Fig. 3A***). The first mutant (TGN46 ΔAAIL) has a shorter TMD (17 amino acids) but keeps the overall amino acid composition, whereas in the second mutant, (TGN46-ST TMD) both the length and composition of the TMD were altered.

First, we expressed different combinations of these proteins in HeLa cells, and monitored their intracellular localization by fluorescence microscopy. Altering the TMD of TGN46 had no discernible impact on intra-Golgi localization (***Fig. 3B*** and ***Fig. S3A***), suggesting that the hydrophobic matching mechanism is not a determinant for intra-Golgi localization of TGN46. Interestingly, even in cells treated with short-chain ceramide (D-ceramide-C6), which causes morphological changes and the physical segregation of the Golgi membranes into distinct ST- and TGN46-positive Golgi subdomains [52–55], no apparent change in the localization of the TGN46 mutants with short TMD with respect to TGN46 WT were observed (***Fig. S4***). However, because our results were obtained using diffraction-limited confocal microscopy (with a spatial lateral resolution ~250 nm), it is still possible that more subtle alterations in the intra-Golgi localization of these mutants would exist at shorter length scales. To address this possibility, we used super-resolution single molecule localization microscopy (SMLM) with a localization accuracy (resolution) of ~15–30 nm. Our results show that, even with this increased spatial resolution, the intra-Golgi localization of the different TGN46 mutants with shorter TMD was indistinguishable from that of TGN46 WT (***Fig. S5***).

Second, we asked whether the TGN46 TMD sequence plays a role in driving transport carrier specificity. Interestingly, the two mutants with shorter TMDs (TGN46 ΔAAIL and TGN46-ST TMD) lost their preference for being co-packaged with PAUF into CARTS, and partially redirect into other transport carriers such as VSVG carriers (***Fig. 3C*** and ***Fig. S3B***).

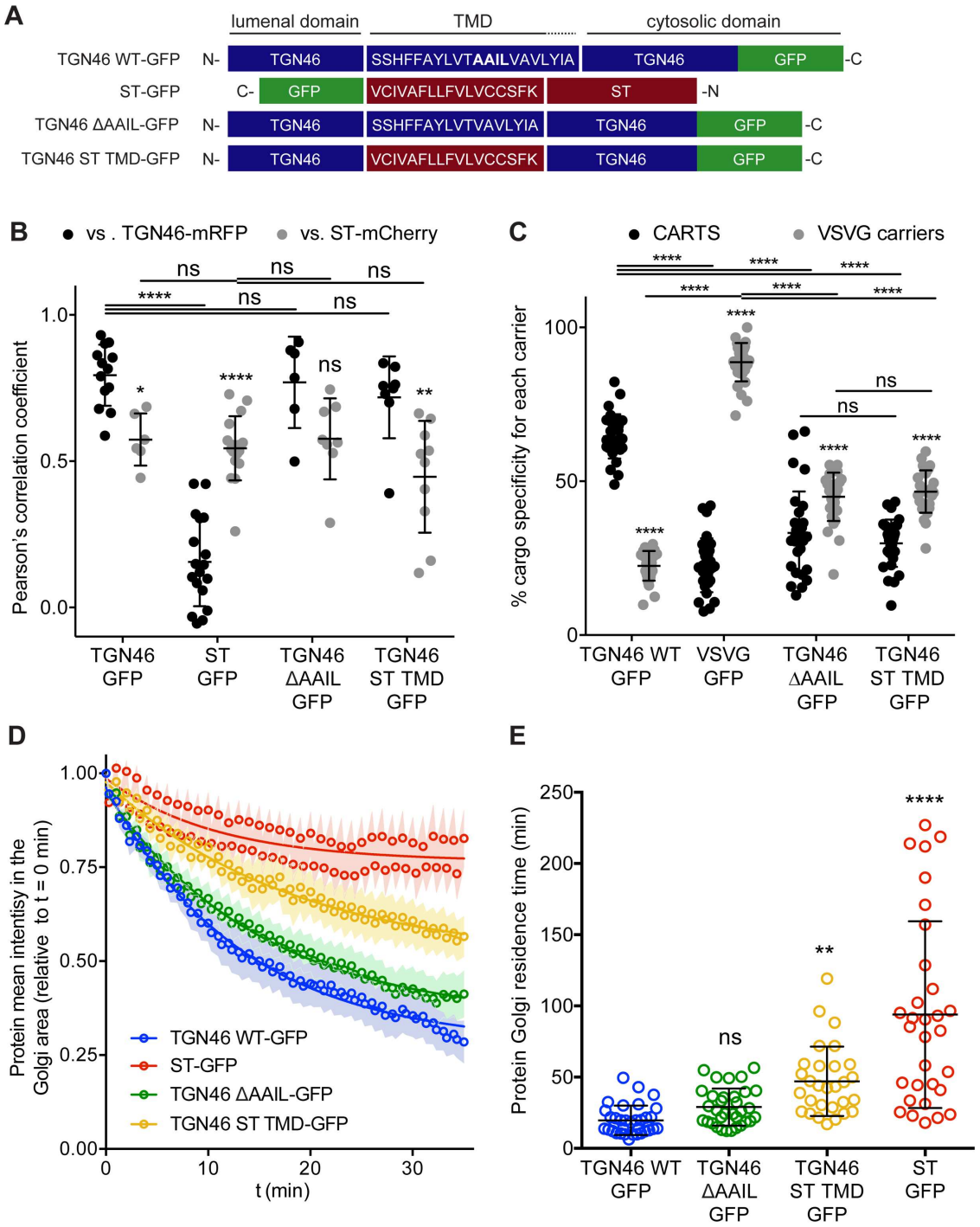


**Figure 3. TGN46 intra-Golgi localization and CARTS specificity are insensitive to TMD length and composition. (A)** Schematic representation of construct domain topology. The amino acid sequence (in the correct topology) of the different transmembrane domains (TMD) is indicated. **(B)** Pearson's correlation coefficient between the perinuclear fluorescence signal of the x-axis indicated proteins with respect to TGN46-mRFP (black symbols) or ST-mCherry (gray symbols), measured from confocal micrographs of HeLa cells expressing the indicated proteins. Results are at least 3 cells from each of n=3 independent experiments (individual values shown, with mean ± stdev). **(C)** Percentage of transport carriers containing each of the cargoes described on the x-axis that are also positive for PAUF (CARTS, black symbols) or VSVG (VSVG carriers, gray symbols), as measured from confocal micrographs of HeLa cells expressing the indicated proteins. Results are from at least 10 cells from each of n=3 independent experiments (individual values shown, with mean ± stdev). **(D)** Relative fluorescence intensity average time trace (mean ± s.e.m.) of FLIP experiments for the indicated proteins. Symbols correspond to actual measurements, solid lines to the fitted exponential decays. **(E)** Residence time in the perinuclear area measured as the half time of the FLIP curves. Results are from from 7–12 cells from each of n=3 independent experiments (individual values shown, with mean ± stdev).

Finally, we investigated how fast these TGN46 mutants with shorter TMDs are exported out of the Golgi apparatus. The FLIP experiments indicated that the chimeric protein TGN46-ST TMD-GFP has a slower Golgi export rate (longer Golgi residence time) as compared to wild type TGN46-GFP. In addition, TGN46-ΔAAIL-GFP was exported at a slightly slower rate, although this difference was not statistically significant (***Fig. 3D, E*** and ***Fig. S3C***). Next, we co-overexpressed TGN46 WT-GFP together with TGN46-ST TMD-mRFP or TGN46 WT-mRFP, as a control, and performed FLIP experiments to measure the rate of TGN46 WT-GFP export with the aim of testing if the expression of these mutants leads to defects in CARTS biogenesis. The results of these experiments show that the Golgi residence time of TGN46 WT-GFP was not affected by the co-expression of either the WT or the chimeric proteins (***Fig. S6A,B***). These data provide further support to the idea that the slower Golgi export rate of TGN46 mutants with short TMDs is a consequence of their compromised selective sorting into CARTS.

It has been reported that some medial Golgi enzymes can dimerize or oligomerize and that this property (kin recognition) is important for TM protein localization along the Golgi stack [41,42,56]. However, there are reports showing that kin recognition is not relevant for ST or for other *trans*-Golgi membrane proteins [48]. To examine if the unaltered intra-Golgi localization of TGN46 ΔAAIL and TGN46-ST TMD compared to WT was due to protein dimerization/oligomerization, we tested whether TGN46-GFP and TGN46-mRFP co-immunoprecipitated when expressed in HeLa cells. Our results show no obvious dimerization between TGN46-GFP and TGN46-mRFP (***Fig. S6C***). Additionally, we also investigated if the shortening of the TGN46 TMD could be altering its glycosylation status. Since TGN46 is sialylated at the *trans*-Golgi cisternae by ST, we tested whether TGN46-ΔAAIL reaches the *trans*-Golgi membranes by monitoring its level of sialylation. HeLa cells expressing TGN46 WT-GFP or TGN46-ΔAAIL-GFP were lysed and the lysates were incubated in the presence or absence of neuraminidase – an enzyme that removes sialic acid –, after which the apparent molecular weight of the different TGN46 mutants was analyzed by western blotting with an anti-GFP antibody. The mutant showed a similar level of sensitivity to neuraminidase digestion as compared to wild-type TGN46 (***Fig. S6D***), suggesting that the length of the TMD of TGN46 does not affect its ability to functionally interact with *trans*-Golgi resident enzymes.

One of the possible consequences of shortening the TMD of TGN46 might be the partial burial of the highly charged residues of TGN46 cytosolic tail into the cytosolic leaflet of the TGN membrane, which, concomitantly, could negatively affect CARTS-mediated export. If so, the observed phenotype would follow from the unnatural proximity of the cytosolic tail to the membrane rather than from a direct effect due to hydrophobic mismatch. To test this hypothesis, we deleted the cytosolic tail of TGN46-ST TMD – which, as we showed earlier (***Fig. 2***), has

no major effect in TGN46 export in CARTS – to generate a mutant with TGN46 lumenal domain and ST TMD (TGN46lum-ST TMD, ***Fig. 2A***). This chimeric protein phenocopies GFP-TGN46 LT with regard to *(i)* their intra-Golgi localization (***Fig. 2B*** and ***Fig. S2A***), and *(ii)* their CARTS specificity (***Fig. 2C*** and ***Fig. S2B***), with only a milder reduction in the Golgi export rate (***Fig. 2D,E*** and ***Fig. S2C***). Taken together, these results strongly indicate that the hydrophobic matching mechanism (as well as the information encoded in the TMD) plays, at most, a secondary role in driving the intra-Golgi localization and Golgi export of TGN46.

**The lumenal domain of TGN46 is necessary and sufficient for its CARTS-mediated export from the TGN**

Finally, we enquired if the lumenal domain of TGN46 plays a role in intra-Golgi localization, Golgi export rate (residence time), and its selective sorting into CARTS. First, we aimed to test whether the lumenal domain of TGN46 is *necessary* for its sorting and packaging into CARTS. We thus generated a deletion mutant of TGN46 lacking its lumenal domain (TGN46 TC) (***Fig. 4A***), expressed it in cells, and monitored its intra-Golgi localization by fluorescence microscopy. GFP-TGN46 TC lost the characteristic intra-Golgi localization of the wild type protein and rather localized in ST-mCherry-positive processing domains of the *trans*-Golgi membranes (***Fig. 4B*** and ***Fig. S5A***). Notably, this exclusion from TGN export domains paralleled a striking reduction in the selective incorporation of GFP-TGN46 TC into CARTS (***Fig. 4D*** and ***Fig. S6A***), as well as in the rate of Golgi export (***Fig. 4F*** and ***Fig. S7A,C***), as compared to the wild type protein. These results consistently indicate that the lumenal domain of TGN46 is *necessary* for CARTS-mediated export of TGN46, therefore suggesting that a signal for sorting and/or packaging into CARTS is contained in this lumenal domain.

Next, we asked whether the TGN46 lumenal domain is *sufficient* for CARTS-mediated TGN exit. We started by generating a soluble cargo protein that only contains the lumenal domain of TGN46 (TGN46lum), tagged with GFP at the N terminus just after the signal sequence (***Fig. 4A***). Upon expression in HeLa cells, GFP-TGN46lum localizes to the Golgi apparatus where it only shows a partial colocalization with TGN46-mRFP and ST-mCherry within the Golgi (***Fig. 4B*** and ***Fig. S5A***), as could be expected when comparing the localization of soluble and TM proteins. Nonetheless, when we used our synchronized cargo release assay to measure selective incorporation into CARTS, GFP-TGN46lum maintained specificity for CARTS-mediated export (***Fig. F4D*** and ***Fig. S6A***). Moreover, FLIP experiments revealed that GFP-TGN46lum exits as fast, or even faster, as GFP-TGN46 WT (***Fig. 4E*** and ***Fig. S7A,B***). We next asked if the information encoded in the TGN46 lumenal domain is by itself able to re-route other proteins into CARTS. In particular, we tested whether TGN46 lumenal domain can lead to CARTS-mediated export of *(i)* a Golgi-resident TM protein (ST), and *(ii)* a CARTS-

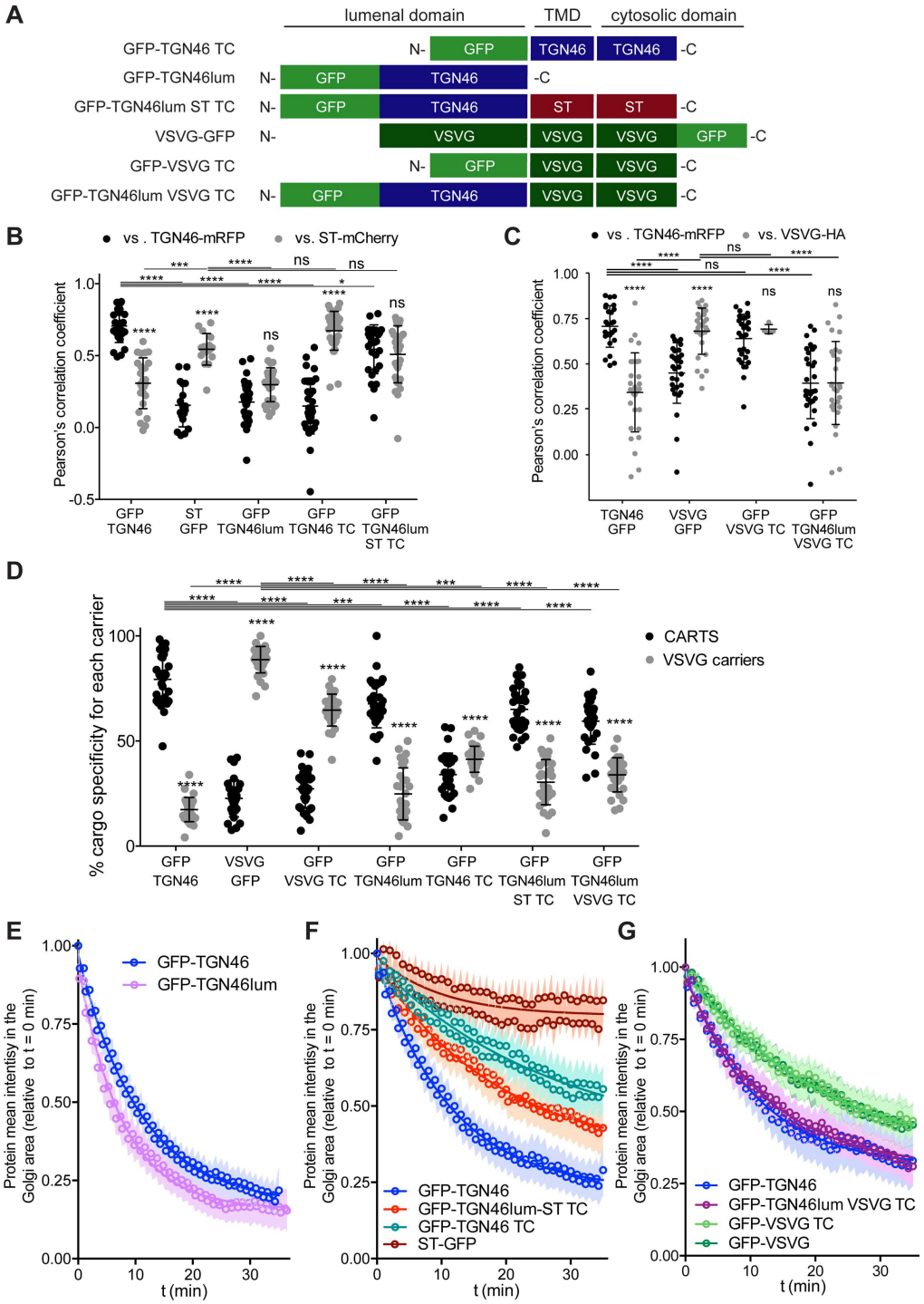


**Figure 4. The lumenal domain of TGN46 is necessary and sufficient for its CARTS-mediated export from the TGN.** **(A)** Schematic representation of construct domain topology. TMD: transmembrane domain. **(B)** Pearson's correlation coefficient between the perinuclear fluorescence signal of the x-axis indicated proteins with respect to TGN46-mRFP (black symbols) or ST-mCherry (gray symbols), measured from confocal micrographs of HeLa cells expressing the indicated proteins. Results are from at least 10 cells from each of n=3 independent experiments (individual values shown, with mean ± stdev). **(C)** Pearson's correlation coefficient between the perinuclear fluorescence signal of the x-axis-indicated proteins with respect to TGN46-mRFP (black symbols) or VSVG-HA (gray symbols; detected by immunofluorescence using an Alexa Fluor 647-conjugated secondary antibody), measured from confocal micrographs of HeLa cells expressing the indicated proteins. Results are from at least 10 cells from each of n=3 independent experiments (individual values shown, with mean ± stdev). **(D)** Percentage of transport carriers containing each of the cargoes described on the x-axis that are also positive for PAUF (CARTS, black symbols) or VSVG (VSVG carriers, gray symbols), as measured from confocal micrographs of HeLa cells expressing the indicated proteins. Results are from at least 10 cells from each of n=3 independent experiments (individual values shown, with mean ± stdev). **(E–G)** Relative fluorescence intensity average time trace (mean ± s.e.m.) of FLIP experiments for the indicated proteins. Symbols correspond to actual measurements, solid lines to the fitted exponential decays.

independent TM cargo protein (VSVG). To that end, we exchanged the lumenal domains (maintaining the correct topology) of ST and VSVG for that of TGN46, thereby generating two chimeric constructs: TGN46lum ST TC, and TGN46lum VSVG TC, respectively (***Fig. 4A***). We then studied the intra-Golgi localization, CARTS-mediated export selectivity, and Golgi export rate of these proteins in relation to their wild type counterparts. Our results indicate that GFP-TGN46lum ST TC maintained a good degree of colocalization with ST-mCherry and additionally it increased its colocalization with TGN46-mRFP (***Fig. 4B*** and ***Fig. S7A***). Similar results were obtained for the intra-Golgi localization of GFP-TGN46lum VSVG TC with respect to TGN46 WT-mRFP and VSVG-HA (***Fig. 4C*** and ***Fig. S7B***). In this case, we also included GFP-VSVG TC – a deletion mutant of VSVG lacking the lumenal domain – as an additional control to remove any possible source of intra-Golgi sorting signals residing in the lumenal region of VSVG. This construct shows a reduced colocalization with respect to both TGN46 WT-mRFP and VSVG-HA, possibly indicating a tug-of-war between lumenal signals – driving localization towards TGN46-positive export domains – and TM/cytosolic signals – driving localization towards VSVG-positive export domains (***Fig. 4C*** and ***Fig. S7B***). Despite these subtle differences in their intra-Golgi localization, the GFP-TGN46lum VSVG TC chimera is specifically exported from the TGN in CARTS, with a similar specificity to that of TGN46-GFP, whereas GFP-VSVG TC is exported by VSVG carriers, similarly to VSVG-GFP (***Fig. 4D*** and ***Fig. S8A***). In line with these observations, FLIP microscopy showed a fast Golgi export rate of GFP-TGN46lum VSVG TC, indistinguishable from that of GFP-TGN46 WT, and a somewhat slower export rate for both GFP-VSVG TC and VSVG-GFP (***Fig. 4F,G*** and ***Fig. S9A,C,D***). These results indicate that the lumenal domain of TGN46 can re-direct other TM cargo proteins into CARTS, thereby acting as a gain-of-function domain for fast export in CARTS out of the Golgi apparatus. Similarly, fusing the lumenal domain of TGN46 to ST also created a protein that is able to be exported out of the TGN by being specifically sorted into CARTS (***Fig. 4D*** and ***Fig. S8A***). Remarkably, TGN46lum ST TC has a shorter Golgi residence time as compared to ST-GFP, with an export rate slightly slower but comparable to that of GFP-TGN46 WT (***Fig. 4F*** and ***Fig. S9A***). Altogether, these results indicate that, as long as the protein is correctly localized, the information encoded in the lumenal domain of TGN46 is not only necessary, but also *sufficient* for its sorting into CARTS for Golgi export.

Lastly, we asked if the lumenal domain of TGN46 can still be properly glycosylated when fused to other proteins. For this, HeLa cells expressing GFP-TGN46 WT, GFP-TGN46lum, GFP-TGN46lum ST TC, or GFP-TGN46lum VSVG TC were lysed and the lysates were incubated in the presence or absence of neuraminidase, after which the apparent molecular weight of the different TGN46 mutants was analyzed by western blotting with an anti-GFP antibody. Our

results indicate a certain degree of sensitivity to neuraminidase digestion, comparable to that of GFP-TGN46 WT (***Fig. S9E***).

**CARTS specificity of cargo proteins correlates with their Golgi export rate**

Our data thus far suggest that cargoes with a high specificity for the CARTS pathway have a relatively fast Golgi export rate (***Figs. 2–4***). To quantitatively illustrate these findings, we plotted the CARTS specificity as a function of the Golgi residence time, for each of the tested cargo proteins. The plots reveal the existence of a negative correlation between CARTS specificity and Golgi residence time (slope~-0.9±0.4% $min^{-1}$, $r^2$~0.4) (***Fig. 5A***). Both TGN46 WT (***Fig. 5A***, dark green) and the different chimeric cargo proteins that contain the lumenal domain but not the cytosolic tail of TGN46 (***Fig. 5A***, light green) are selectively sorted into CARTS (>50% specificity) and rapidly exported out of the Golgi (short Golgi residence times ~10–30 min). Interestingly, in the absence of the lumenal domain of TGN46 (***Fig. 5A***, red) or when only the TMD sequence of TGN46 is altered (while keeping the WT cytosolic tail) (***Fig. 5A***, yellow), cargoes lost CARTS specificity (<35%) with the concomitant decrease in the Golgi export rate (larger Golgi residence times ~30–50 min). Finally, VSVG (***Fig. 5A***, blue), which is a cargo that is excluded from CARTS [33], shows a slower Golgi export rate (Golgi residence time ~30 min), which indicates that VSVG-containing carriers mediate a relatively slower Golgi export route as compared to CARTS, thereby underscoring the different export kinetics of distinct Golgi export routes.

**The cargo sorting function of TGN46 is mediated by its lumenal domain**

TGN46 is a bona fide CARTS component [2], and our data indicate that it is required for PAUF sorting into CARTS for secretion (***Fig. 1***). Furthermore, we have shown that the lumenal domain of TGN46 is necessary and sufficient for the incorporation of this TM protein into CARTS (***Fig. 4***). It is therefore possible that TGN46 mediates the sorting of its client cargoes by means of its lumenal domain. To test this hypothesis, we investigated whether the expression of different mutants of TGN46 would rescue the sorting and export defect observed in TGN46-KO cells. In particular, we studied the following TGN46-based proteins: GFP-TGN46 WT (wild type protein), GFP-TGN46 LT (no cytosolic tail), GFP-TGN46 ST TMD (TGN46 with the shorter TMD of the Golgi resident ST), and GFP-TGN46 TC (no lumenal domain). First, TGN46-KO HeLa cells co-expressing any of these TGN46 constructs together with PAUF-mRFP or VSVG-HA were synchronized by a 20º block and 15 min release, after which the cells were fixed and prepared for fluorescence microscopy (***Fig. S10***). We quantified the percentage of carriers containing the different TGN46 mutants that were also positive for either PAUF (CARTS marker) or VSVG (non-CARTS marker) and compared those to the distributions found when the same proteins were expressed in the parental HeLa cells (***Fig. 5B***;

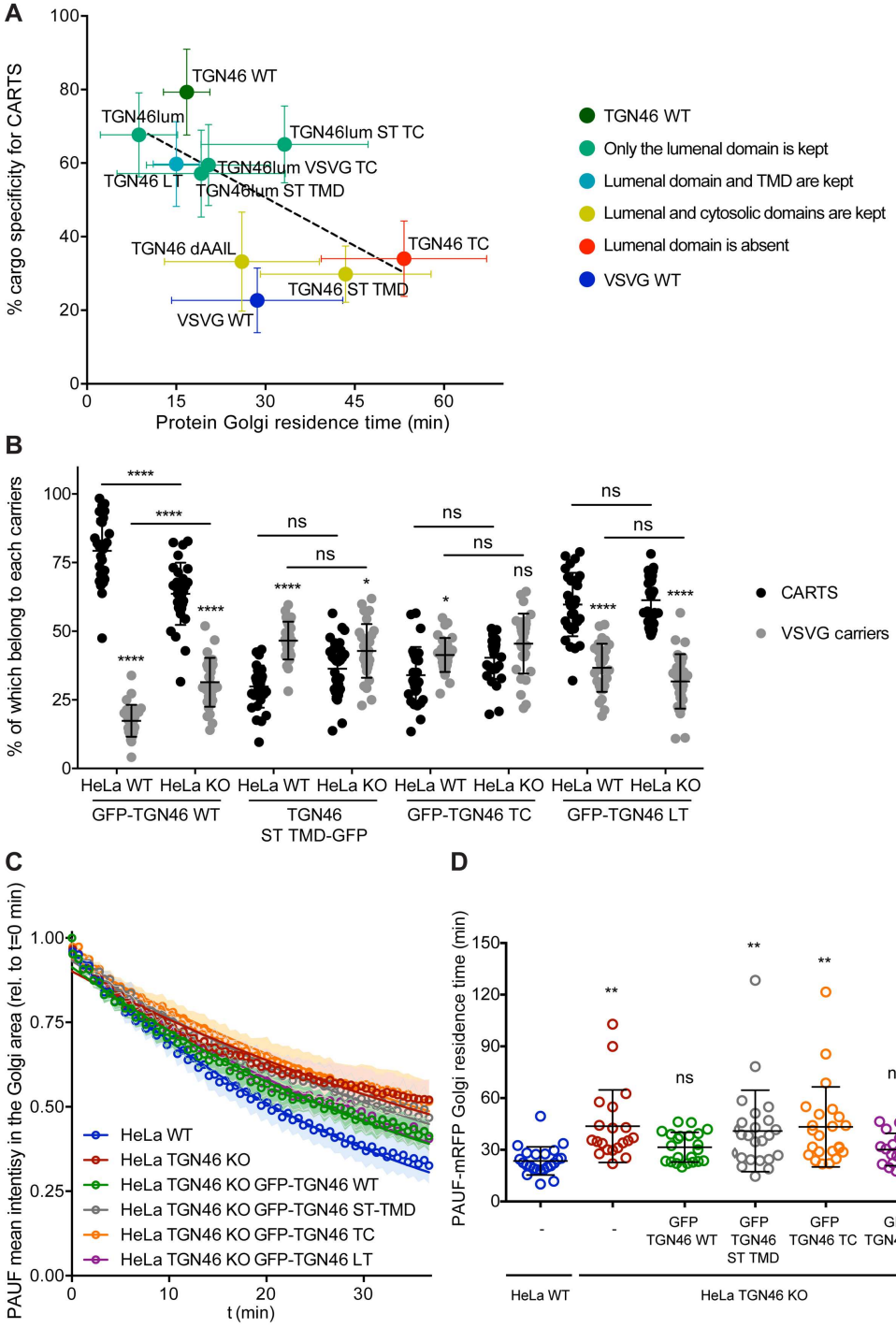


**Figure 5. The cargo sorting function of TGN46 is mediated by its lumenal domain. (A)** CARTS specificity of cargo proteins correlates with their Golgi export rate. Plot of the percentage of cargo-positive vesicles that are also positive for PAUF (CARTS marker) as a function of the Golgi residence time as measured from FLIP experiments, for the different indicated cargo proteins (color coding explained in the legend on the right). Dashed black line represents a linear fit of the data points (shown as mean ± s.e.m.), where the slope is statistically different from zero (extra sum-of-squares F test, p value= 0.04). **(B)** Percentage of transport carriers containing each of the cargoes described on the x-axis that are also positive for PAUF (CARTS, black symbols) or VSVG (VSVG carriers, gray symbols), as measured from confocal micrographs of HeLa cells (either WT or TGN46 KO cell lines) expressing the indicated proteins. Results are at least 10 cells from each of n=3 independent experiment (individual values shown, with mean ± stdev). **(C)** Relative fluorescence intensity average time trace (mean ± s.e.m.) of FLIP experiments for the indicated proteins expressed in HeLa WT or HeLa TGN46 KO cells, as detailed in the legend. Symbols correspond to actual measurements, solid lines to the fitted exponential decays. **(D)** Residence time of PAUF-mRFP in the perinuclear area of HeLa cells (WT or KO), expressing the different proteins as labeled in the x axis, and measured as the half time of the FLIP curves. Results are from 7–12 cells from each of n=3 independent experiments (individual values shown, with mean ± stdev).

see also ***Fig. 2C, 3C, 4D***). These results indicate that CARTS selectivity of these cargo proteins was not severely altered in the TGN46 KO cells as compared to the parental cell line. Next, we carried out FLIP experiments in TGN46-KO cells that were transiently expressing PAUF-mRFP together with GFP-TGN46 WT, GFP-TGN46 LT, GFP-TGN46 ST TMD, or GFP-TGN46 TC and measured the rate of PAUF-mRFP export from the Golgi. Interestingly, overexpression of GFP-TGN46 WT or GFP-TGN46 LT – but not of GFP-TGN46 ST TMD or GFP-TGN46 TC – was able to rescue PAUF-mRFP export from the Golgi in TGN46-KO cells (***Figs. 5C,D*** and ***S11***). Taken our data together, we propose a model in which the proper partitioning of TGN46 into TGN export domains (CARTS formation sites) is required for its lumenal domain to efficiently recruit and sort PAUF and other CARTS cargoes into nascent transport carriers.

**The lumenal domain of TGN46 forms liquid droplets by liquid-liquid phase separation *in vitro***

Our data suggest that the lumenal domain of TGN46 might have a propensity to self-associate, because *(i)* the steady-state intra-Golgi localization of TGN46 is lost when the lumenal domain is deleted, (***Fig. 4B*** and ***Fig. S7A***); and *(ii)* although the soluble lumenal domain of TGN46 showed an intermediate intra-Golgi localization phenotype, anchoring this domain to the membrane by fusing it to the *trans*-Golgi-targeting sequence of ST conferred this chimera a localization pattern indistinguishable from that of full length TGN46 (***Fig. 4B*** and ***Fig. S7A***). To obtain insights on how this might occur, we analyzed the sequence features of this domain (***Fig. S12A***). On the one hand, TGN46 is a heavily glycosylated protein, including 9 predicted *N*-linked glycosylation sites, multiple *O*-linked glycosylation sites, as well as 5 phosphosites (***Fig. S12B***), all of them located at the lumenal domain. Structurally, this region is highly disordered, as evidenced by a high PONDR score (in the range 0.5–1) for most of its amino acid sequence (***Fig. S12C***), indicating with high probability that the lumenal domain of TGN46 is essentially intrinsically disordered (ID). In recent years, ID regions of various proteins have been shown to have the capacity to form biomolecular condensates by a physical mechanism known as liquid-liquid phase separation (LLPS) [57–62]. Due to their liquid nature, these condensates take spherical shapes, and their components are mobile within the condensate (dense phase) and can also exchange with those present, at a lower concentration, in the external solution (light phase). We thus tested whether the TGN46 lumenal domain has the capacity to undergo LLPS *in vitro*. We purified the protein domain (amino acids 1–437) fused to GFP in *E. coli* and assessed by fluorescence microscopy the formation of liquid droplets upon protein concentration increase and addition of Ficoll – a well-known crowding agent used to mimic the crowded environment of the Golgi lumen. Our results indicate that, when present at a high concentration (100 μM) and in the presence of Ficoll, TGN46-lumenal is able to form spherical

structures of a range of sizes (~1 μm), characteristic of biomolecular condensates (***Fig 6A***). Notably, time-lapse fluorescence microscopy imaging revealed fusion events between condensates, which is indicative of their liquid nature (***Fig. 6B***). In addition, we carried out fluorescence recovery after photobleaching (FRAP) experiments to determine whether protein molecules could diffuse inside the condensates. Our results indicate that, indeed, protein molecules diffuse within the dense phase and that the fluorescence recovers with a characteristic half-time of 4.46±1.54 s, and a mobile fraction (MF) of 0.70±0.11 (***Fig. 6C***); we also performed FRAP experiments where an entire droplet was bleached and observed fluorescence recovery indicating that protein molecules do exchange between the light and dense phases (***Fig. 6D***). Together, these results show the capacity of the TGN46 lumenal domain to form liquid droplets by LLPS *in vitro*. We further characterized the driving forces for this process by assessing the effect of solution conditions on phase separation. We first studied the effect of addition of NaCl to the samples (***Fig. 6E***), and found that this decreases the propensity of the domain to phase separate, indicating that LLPS is favored at low ionic strength. These data suggest that the interactions stabilizing the droplets formed by TGN46 are of electrostatic nature, between amino acid side chains of opposite charge or hydrogen bonds. This behavior is in agreement with a clear bias in the residue type composition of the domain, that is highly enriched in Lys and Glu relative to a typical ID domain as defined by the DisProt 3.4 database (***Fig. S12D–F***). Finally, we assessed the effect of temperature on LLPS by measuring the apparent absorbance, *i.e.,* the turbidity, of the same samples at 20, 40 and 60 ºC (***Fig. 6F***), and obtained that LLPS is promoted at high temperatures, in the lower critical solution temperature (LCST) regime, indicating that LLPS of the domain *in vitro* is entropy-driven. Taken together, our data reveal that the lumenal domain of TGN46, which is crucial for its cargo sorting function, has the capacity to form liquid droplets by LLPS *in vitro*, thereby suggesting a possible biophysical mechanism for how this TM protein mediates the sorting of secretory cargoes into transport carriers for their secretion.

## DISCUSSION

### TGN46 is necessary for cargo loading into CARTS

Here, we revealed a novel role for TGN46 in the sorting the secretory cargo protein PAUF into nascent transport carriers at the TGN. CRISPR/Cas9-edited HeLa cells lacking TGN46 showed *(i)* a drastic inhibition in PAUF secretion (***Fig. 1A***); *(ii)* a reduction in the number of cytoplasmic CARTS – but not of other TGN-to-plasma membrane carriers such as VSVG carriers – (***Fig. 1B***); and *(iii)* a decrease in the Golgi export rate of PAUF (***Fig. 1C,D***). To investigate the role of TGN46 in cargo sorting into nascent transport carriers, we took

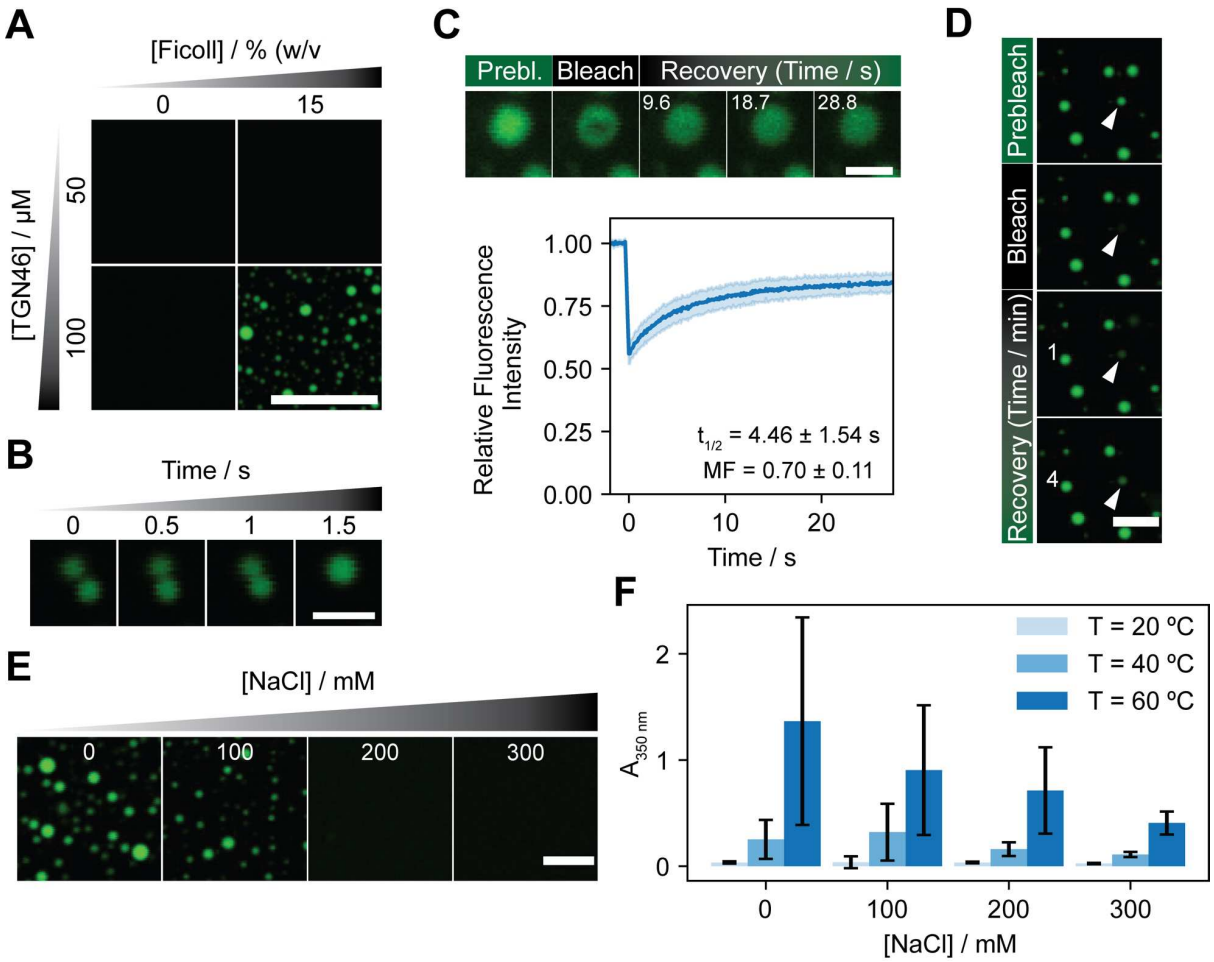


**Figure 6.** ***In vitro*** **characterization of TGN46 lumenal domain LLPS. (A)** Fluorescence microscopy images of 50 and 100 µM protein concentration with 0 and 15 % (w/v) Ficoll 70 at 40 ºC. Scale bar represents 10 µm. **(B)** Example of a fusion event. Scale bar represents 2 µm. **(C)** FRAP experiment showing recovery after photobleaching within a single droplet. Scale bar represents 2 µm. The FRAP curve shown as the mean and standard deviation of 20 independent measurements and the corresponding fitted values are shown in the bottom plot. **(D)** FRAP experiment showing recovery after photobleaching of an entire droplet. Scale bar represents 5 µm. **(E)** Fluorescence microscopy images at different ionic strengths (0, 100, 200 and 300 mM NaCl) of a 100 µM TGN46lum sample with 15 %(w/v) Ficoll 70 at 40 ºC. Scale bar represents 5 µm. **(F)** Apparent absorbance measurements at 350 nm of the same samples as **(E)** at temperatures of 20, 40 and 60 ºC.

advantage of the phenotype caused by the exogeneous expression of PKD-KD, which consists in the presence of long, cargo-containing tubules emanating from the TGN membranes [40]. Because these tubules are fission-defective transport carriers, and membrane fission is downstream of cargo sorting, we can use this assay as a useful approach to investigate cargo sorting into PKD-dependent transport carriers at the TGN. Our results highlighted the need for TGN46 to sort and package the secretory cargo PAUF into PKD-KD-induced TGN tubules (***Fig. 1E***), therefore suggesting a prime role of TGN46 in cargo sorting. Indeed, TGN46 – as well as its rodent orthologs TGN38/TGN41 – shares the characteristics of a typical cargo receptor: it is a type-I single-pass TM protein that cycles between the TGN and the plasma membrane, which led to the suggestion of TGN46 being a putative cargo receptor [22]. Cargo receptors usually exhibit a high binding affinity to their clients; however, our data suggest the possibility that TGN46 can incorporate cargo proteins by a lower affinity LLPS-like condensation mechanism. Although future work will be necessary to pinpoint the mechanism that TGN46 uses for cargo sorting and loading into carriers, we believe that the data reported here shed some light into the actual role of human TGN46 for the sorting and loading of cargo proteins into TGN-derived transport carriers destined to the cell surface.

Although we focused on the study of the model CARTS cargo protein PAUF, it seems reasonable to expect that TGN46 is responsible for the sorting of other cargoes into transport carriers at the TGN. Interestingly, the lumenal domain of TGN38 has been shown to interact with the adhesion receptor integrin ß$_1$ and to partially co-localize with integrins $\alpha_5$ and ß$_1$, but not $\alpha_V$ or ß$_3$ [27]. In addition, TGN38 regulates cell adhesion, as the overexpression of TGN38 leads to cell detachment from the substrate [26,28,32,63,64]. Remarkably, integrin ß$_1$ is transported from the TGN to the cell surface in a Rab6-mediated [65] and PKD-dependent manner [66]. Because TGN46 binds a cytosolic protein complex made of 62 kDa protein (p62) and Rab6 [23], and CARTS are PKD-dependent transport carriers that share many similarities with Rab6-positive carriers [2], we propose that the observed role of TGN46 as a cargo receptor for the sorting of the soluble CARTS-specific cargo PAUF is quite general, and can include a long list of both soluble and TM cargo proteins, such as $\alpha_5$ß$_1$ integrins. Further work will be required to grasp the full magnitude of the role of TGN46 in protein sorting for export and secretion out of the TGN.

**TGN46 localization to *trans*-Golgi membranes is independent of TMD length and composition**

Different mechanisms have been proposed to dictate the spatial and temporal organization of Golgi residents (e.g., glycosylation enzymes) and their respective substrates (e.g., secretory cargoes) [41,42,56]. Amongst these, a lipid-based retention/sorting mechanism has been proposed for Golgi TM proteins [38,46–48,67]. This mechanism builds on the observation that the levels of

certain lipids, such as cholesterol and SM, are enriched along the *cis*- to *trans*- axis of the Golgi stack [68,69]. This lipid gradient correlates with an increase in the thickness of those membranes [49]. In addition, a comprehensive bioinformatic study using large datasets of TM proteins from different organisms showed a correlation between the intracellular localization of these proteins and different specific features of their TMDs, such as their length, which on average is shorter for proteins of the early secretory pathway as compared to those of the late secretory pathway [47]. Moreover, it has been proposed that not only the length of the TMD but the distribution of bulky and highly hydrophobic amino acids within the TMD are also important factors for specific location of TM proteins [47,50]. Altogether, these studies have led to the suggestion of the hydrophobic matching model, which proposes that gradients in bilayer thickness along the membranes of the secretory pathway contribute/drive the sorting and retention of TM proteins across the secretory pathway. Although there is compelling evidence for a TMD-based mechanism for targeting certain TM proteins to specific cell surface domains [70], to localize type-II resident proteins of the cell surface and the Golgi membranes [48,50], and also to sort the type-III TM protein linker for activation of T-cells (LAT) by raft-mediated partitioning [71,72], it remained unclear how this mechanism contributed to the retention, sorting and lateral segregation of Golgi resident enzymes and their substrates. Interestingly, by using a coarse-grained mathematical model of intra-Golgi transport, Dmitrieff et al. showed that experimental data on the Golgi dynamics of secretory cargoes and Golgi residents cannot be explained if the hydrophobic matching mechanism is the sole retention mechanism for Golgi residents [73]. In agreement with this latter proposal, our results revealed that hydrophobic mismatch between TMDs and bilayer thickness is not sufficient to drive the sorting of a TM Golgi-resident enzymes from substrate cargoes along the *trans*-Golgi/TGN membranes. Specifically, we studied the role of TMD length and amino acid composition in intra-Golgi localization of the type-I single-pass TM cargo glycoprotein TGN46, and observed that localization and sialylation of TGN46 is not affected when its TMD is shortened or even replaced by that of the Golgi-resident type-II TM enzyme ST (***Fig. 3A,B*** and ***Fig. S3A***). These data suggest that the hydrophobic length and amino acid composition of the TMD of TGN46 is not a major contributing factor to localize this TM into Golgi export domains for its function in sorting and packaging of soluble cargoes into nascent CARTS.

**A role for the cytosolic tail of TGN46 in driving its proper intra-Golgi localization**

Our results indicate that the cytosolic tail of TGN46 contains a specific signal allowing the perinuclear pool of TGN46 to localize in the right sub-compartment within the TGN membranes. In particular, the localization of a TGN46 mutant lacking the cytosolic tail was shifted towards Golgi processing domains (ST enzyme-positive regions) rather than in export domains (TGN46 WT-positive regions) (***Fig. 2B*** and ***Fig. S2A***). It has been well documented

that the cytosolic tail of TGN38 – the rodent ortholog of TGN46 – contains a tyrosine-based motif for internalization and recycling of the protein back to the TGN [29,32]. Adding to these earlier reports, our data suggest that the cytosolic tail of TGN46 also determines its fine intra-Golgi localization. Factors such as Vps74/GOLPH3 or coat proteins such as COPI [74–76], influence enzyme-cargo interaction/segregation by recognizing cytoplasmic signals and thereby inducing protein retention by fast recycling. In addition, SM metabolism can also contribute to laterally organize the Golgi membranes at the nanoscale for efficient cargo-enzyme interactions [52,53].

**Cargoes destined for secretion exit the Golgi with different export rates**

We observed that the Golgi residence time of different TGN46-based chimeric proteins was different depending on the specific export route they take for the TGN export (***Fig. 5A***). In particular, when we compared the export rate of two different PKD-dependent transmembrane cargo proteins (TGN46, which is exported in CARTS; and VSVG, which is not), we found that CARTS appear to be a faster export route (~15 min Golgi residence time) than VSVG carriers (~30 min Golgi residence time) (***Fig. 5A***). Remarkably, when we generated a series of chimeras combining different domains from different proteins, we observed that loss of CARTS specificity correlated with larger residence times in the Golgi apparatus (***Fig. 5A***). These results could explain why cells use different routes (with different machineries) for the export of secretory or TM cargo proteins to the same destination, *i.e.*, different cargoes might require longer/shorter residence times in the Golgi and/or faster transport kinetics to the cell surface. It is possible that developing various TGN-to-plasma membrane export routes of different kinetics might have endowed cells with beneficial mechanisms to cope with their secretory needs under stress conditions.

CARTS have been suggested to be enriched in cholesterol and SM [2,77], and their biogenesis to require intact ER-Golgi membrane contact sites (MCS) supplying the TGN with these lipids (or their precursors) [77,78]. Notably, data from Deng, Pakdel et al. suggested that TGN46 is a native cargo of the SM-dependent TGN export pathway, as it was identified by mass spectrometry of to be co-packaged in carriers containing the lumenal SM sensor EQ-SM-APEX2 [20]. Given the similarities between the SM/Cab45 and CARTS export pathways [1,2], it is tempting to speculate that TGN46 could be enriched in ER-Golgi MCS and perhaps complement the sorting function of Cab45 for a subset of secretory cargo proteins.

Further elaborating on these specific needs/characteristics of different cargoes/export routes will be of outmost importance in the future to better understand the intricate relationships between physiological needs and the regulation of the secretory machinery of the cell [2,5,79,80].

**Formation of liquid biomolecular condensates as a possible cargo sorting mechanism at the TGN**

Our *in vitro* data show that the lumenal domain of TGN46 has the capacity to form liquid droplets by LLPS (***Fig. 6***). Specifically, we observed that LLPS of TGN46 lumenal domain is promoted at relatively high protein concentration (100 μM) and in the presence of the crowding agent Ficoll. These conditions might seem at first glance somewhat extreme, however, we need to stress the fact that TGN46 is a TM protein. LLPS of TM proteins can be assisted by a local nucleation that leads to a locally very high protein concentration [58,62]. TGN46 is a highly abundant protein, its copy numbers have been estimated to be ~30,000 in a typical HeLa cell [81]. Given that the vast majority of TGN46 is in the TGN at steady state, we can estimate the local concentration of TGN46 – considering a total TGN volume of ~100–500 $\mu m^3$ (Ref. [82]) – to be ~100–500 μM. Hence, our *in vitro* results match well the requirement for TGN-specific LLPS. Importantly, if TGN46 were to phase separate at lower concentrations, it could potentially form condensates at the ER, but no function has been described for TGN46 in that organelle. Interestingly, the levels of the cation-dependent mannose 6-phosphate receptor – a well-known cargo receptor at the TGN for the sorting of lysosomal hydrolases into clathrin-coated vesicles – are about 10-fold higher than those of TGN46: ~200,000 copies per HeLa cell [81]. Of notice, our co-immunoprecipitation experiments showed no evidence for strong TGN46-TGN46 protein interactions (***Fig. S6C***), which agrees with our suggestion that TGN46 forms liquid condensates that are stabilized by weak interactions. It seems therefore reasonable to propose that the mechanism of cargo sorting by TGN46 might be different from that of a classical cargo receptor, such as the mannose 6-phosphate receptor, which binds its clients in an ~1:1 stoichiometry. It still remains unclear how PAUF is recruited to nascent CARTS by the lumenal domain of TGN46. PAUF is a putative lectin, so it is possible that it interacts with TGN by recognizing the glycans on its lumenal domain (***Fig. S12B***). Alternatively, or in parallel, LLPS of the lumenal domain of TGN46 could create liquid droplets with a specific chemical microenvironment (pH, $Ca^{2+}$ concentration, etc.), which might serve to recruit certain cargoes. Future endeavors along these lines will help elucidate the mechanistic details of cargo sorting by TGN46.

Remarkably, Parchure et al. recently showed that LLPS might also play a dominant role in the formation of secretory insulin-containing granules for regulated exocytosis [83]. The authors showed that the chromogranins – key regulators of secretory granule formation – can undergo LLPS *in vitro* in conditions of low pH, such as the one found in the TGN. Notably, cargoes such as proinsulin or LyzC do co-partition with chromogranins in the liquid condensates, and put forward a "client sponge" model in which secretory cargoes are sorted into liquid biomolecular condensates based on their size. It will be interesting to investigate whether

TGN46 and chromogranins use two parallel LLPS-based pathways for the sorting of different cargoes for constitutive and regulated secretion, respectively.

In summary, we presented here experimental results that support a model in which TGN46 serves as a sorting receptor for a subset of cargoes at the TGN. Thanks to TGN46, these cargoes are sorted packaged into nascent CARTS for their fast delivery to the cell surface or for secretion outside the cell. The sorting capabilities of TGN46 are ascribed to its lumenal domain, an ID region prone to undergo phase separation. Indeed, our *in vitro* results showed that this domain has the capability to form liquid droplets by LLPS. Based on our findings, we propose a working model in which TGN46 forms small liquid condensates at the TGN that serve to recruit secretory cargoes in the lumen of the TGN for their sorting and fast export to the cell surface by CARTS.

## ACKNOWLEDGMENTS

We thank members of the Single Molecule Biophotonics lab at ICFO, Chris Burd, Ivan Castello-Serrano, and Ilya Levental for valuable discussions. We thank Nathalie Brouwers and the Centre for Genomic Regulation/Universitat Pompeu Fabra FACS Unit (Barcelona) for help with cell sorting and the IRB Barcelona Advanced Digital Microscopy (ADM) Core Facility for help with microscopy. We also thank Jordi Andilla and Maria Marsal for technical support at the Super-resolution Light Nanoscopy (SLN) facility at ICFO. The authors acknowledge the Protein Technologies Unit, Centre for Genomic Regulation (CRG) (Barcelona, Spain) for providing the protein used in this study. C.G.-C. acknowledges a FPI fellowship awarded by MINECO in the 2018 call. P.L., X.S., M.F.G.-P. and F.C. acknowledge support from the Government of Spain (FIS2015-63550-R, BFU2015-73288-JIN, FIS2017-89560-R, RYC-2017–22227, PID2019-106232RB-I00/10.13039/501100011033/110198RB-I00 and PID2020-113068RB-I00 / 10.13039/501100011033; Severo Ochoa CEX2019-000910-S), Fundació Privada Cellex, Fundació Privada Mir-Puig, and Generalitat de Catalunya (CERCA, AGAUR), ERC Consolidator Grant CONCERT (GA 648201) and Advanced Grants NANO-MEMEC (GA 788546) and LaserLab 4 Europe (GA 654148).

## AUTHOR CONTRIBUTIONS

Conceptualization, P.L. and F.C.; Methodology, P.L., C.G.-C., Y.W., C.R, X.S., and F.C.; Software, C.R.; Formal analysis, P.L., C.G.-C., Y.W., C.R., X.S., V.M., M.F.G.-P., and F.C.; Investigation, P.L., C.G.-C., Y.W., and F.C.; Writing – Original Draft, P.L. and F.C.; Writing

– Review & Editing, all authors; Funding Acquisition, V.M., X.S., M.F.G.-P., and F.C.; Supervision, X.S., M.F.G.-P., and F.C.

## DECLARATION OF INTERESTS

The authors declare no competing interests

## METHODS

### Reagents and antibodies

Brefeldin-A (BFA), from Sigma-Aldrich, was dissolved in Dimethyl Sulfoxide (DMSO) (Sigma-Aldrich) as a 10 mg/mL stock solution, and used at 5 µg/ml concentration. N-Hexanoyl-D-erythro-sphingosine (D-cer-C6), from Matreya, was dissolved in pure ethanol (Merck) as a 10 mM stock solution, and used at 20 µM concentration. Cycloheximide was purchased from A.G. Scientific, diluted to 1M in DMSO as a stock solution, and used at 100 µM concentration. Ficoll 70 was purchased from Sigma-Aldrich and dissolved in water to a 64% (w/v) as a stock solution. NaCl was obtained from Melford. For the coating of the slides, toluene was used from PanReac, ethanol from Scharlau and 3-[methoxy(polyethyleneoxy)propyl]trimethoxysilane (CAS 65994-07-2) from acbr GmbH. Sheep anti-human TGN46 was from AbD Serotec. Mouse monoclonal against HA was from Biolegend. Mouse monoclonal against Myc was from Sigma-Aldrich. Rabbit polyclonal antibody against Flag was from Sigma-Aldrich. Rabbit polyclonal antibody against GFP was from Abcam. Alexa Fluor-labeled secondary antibodies were from Invitrogen and HRP-conjugated secondary antibodies from Sigma-Aldrich. For STORM, the activator/reporter dye-conjugated secondary antibodies were in-house-labelled donkey-anti-mouse and donkey-anti-rabbit obtained from ImmunoResearch, used at a final concentration of 20 µg/ml. The dyes used for labelling were NHS ester derivatives: Alexa Fluor 405 Carboxylic Acid Succinimidyl Ester (Invitrogen), Cy3 mono-Reactive Dye Pack (GE HealthCare), and Alexa Fluor 647 Carboxylic Acid succinimidyl Ester (Invitrogen). Antibody labelling reactions were performed as previously reported [88].

### Cell culture, plasmids and siRNA

HeLa cells were cultured in DMEM (Lonza and Capricorn Scientific) containing 10% fetal bovine serum (FBS) (ThermoFisher and Capricorn Scientific), 1% penicillin/streptomycin (Biowest), and 2 mM L-Glutamine (Biowest). Cells were transfected with DNA using Xtreme-GENE 9 DNA (Roche) or with TransIT-HeLaMonster (Mirus) following manufacturer's recommendations. The TGN46-GFP plasmid, which was kindly provided by Dr. S. Ponnambalam (Leeds University, Leeds, England, UK), was generated by inserting human TGN46 cDNA into a pEGFP-N1 vector using the BamHI restriction site. TGN46 ΔAAIL-GFP, TGN46-ST TMD-GFP, GFP-TGN46, GFP-TGN46 LT, GFP-TGN46 TC, GFP-TGN46lum, GFP-TGN46lum-ST TMD, GFP-TGN46lum-ST TC, GFP-TGN46lum-VSVG TC, and GFP-VSVG TC were sub-cloned by Gibson assembly [89] and/or DNA digestion and ligation using TGN46-GFP as a backbone and TGN46-GFP, ST-GFP, or VSVG-GFP as DNA sequence

providers. TGN46-mRFP was generated by Gibson assembly of the KpnI- and EcoRI-digestion of the previously described plasmid PAUF-mRFP [33]. TGN46-ST TMD-mCherry was sub-cloned by Gibson assembly using TGN46-mRFP as the backbone and ST-GFP as DNA sequence providers. PAUF-MycHis and PAUF-mRFP plasmids were described earlier [33]. ST-GFP, which encodes for the initial 45 amino acids of the ST6Gal-I ST, comprising the cytosolic domain, the TMD and 20 amino acids of the lumenal domain, was cloned into pEGFP-N1 as previously described [52]. The ST-mCherry plasmid was generated from the previously described plasmid ST-FKBP-mCherry [90] by Gibson assembly of the BglII- and BamHI-digested plasmid. The VSVG-GFP plasmid was described previously [13]. VSVG-HA was generated by Gibson assembly from VSVG-GFP. PKD2-KD-Flag plasmid was described earlier [91]. pETM14-6his-mGFP -TGN46lum plasmid for bacterial expression was cloned using a synthetic fragment of bacterial optimized TGN46 (gblock IDT), meGFP amplified from GFP-TGN46-lum and assembled in pETM14 backbone vector using Gibson assembly. All plasmids were verified by sequencing (STAB vida). SnapGene software (obtained from GSL Biotech) and ApE software (by M. Wayne Davis) were used for molecular cloning procedures.

For TGN46 transient silencing, HeLa cells were transfected using HiPerFect Transfection Reagent (QIAGEN) with 5 nM of TGN46 siRNA (oligo name: SASI_HS01_00080765, from Sigma-Aldrich), following the manufacturer's recommendations. MISSION siRNA Universal Negative Control #1 was used as a control siRNA. 48h after transfection, corresponding experiments were performed.

Single-clone TGN46 KO HeLa cells were generated by CRISPR/Cas9. HeLa cells were transfected with U6-gDNA (5'-AAAGACGTCCCTAACAAGT-3'; clone ID es: HSPD0000063884): CMV-eCas9-2a-tGFP (Sigma-Aldrich). 48h after transfection, GFP-positive cells were sorted as individual cells by FACS using a BD Influx cell sorter (BD Biosciences). Upon clone expansion, KO effectiveness of the different clones was checked by SDS-PAGE and Western blotting and also by immunofluorescence microscopy.

**Immunofluorescence microscopy**

Samples were fixed with 4% formaldehyde in PBS for 15 min and permeabilized and blocked with 0.2% Triton X-100, 3% BSA in PBS for 30 min prior to antibody staining. Fixed samples were analyzed with a TCS SP8 STED 3X system (Leica) in confocal mode using a 100x 1.4NA objective and HyD detectors. Images were acquired using the Leica LAS X software and converted to TIFF files using ImageJ (version 1.43; National Institutes of Health). Two-channel colocalization analysis was performed using the ImageJ software and the Pearson's correlation coefficient was calculated in a ROI using the "Manders Coefficients" plugin developed at the

Wright Cell Imaging Facility (Toronto, Canada). The ROI was determined as a mask created on the Golgi region formed upon Binary transformation (using the Default Thresholding given by the software) of the sum of both channels. Vesicle colocalization analysis was performed using ImageJ and was calculated using the "Spots colocalization (ComDet)" plugin developed by Eugene A. Katrukha (Utrecht University, Netherlands). Golgi-derived tubules were quantified manually upon Z-projection (maximum intensity) performed using the ImageJ software.

**FLIP microscopy**

Growth media of the HeLa cells seeded on Nunc Lab-Tek 8-wells 1.0 bottom glass chamber slides was supplemented with 25 mM HEPES (pH 7.4) prior to experiment. FLIP experiment was performed on a TCS STED CW system (Leica) in confocal mode using a 63x XNA objective and HyD detectors. Using the Live Data Mode tool of Las AF software (Leica), intermittent bleaching steps were combined with imaging of the whole cell during ~35 min.

When the FLIP experiments were performed on a GFP-containing protein, the series consisted of the following steps: (1) Image 512x512 pixels and pixel size ~75 nm, 200 Hz acquisition speed, 5% nominal power of an Argon Laser (488 nm). (2) Do 6x bleaching steps, keeping the same parameters as in step 1, but with a 100% laser power on a manually selected region encompassing the entire cell except the Golgi region. (3) Repeat step 1. (4) Pause for 40 s. (5) Repeat step 1. (6) Repeat steps 2–5 for 35 times.

When the FLIP experiments were performed on a mRFP-containing protein, the series consisted of the following steps: (1) Image 512x512 pixels and pixel size ~75 nm, 200 Hz acquisition speed, 15% nominal power of a HeNe Laser (543 nm). (2) Do 5x bleaching steps, keeping the same parameters as in step 1, but with a 100% laser power on a manually selected region encompassing the entire cell except the Golgi region. (3) Repeat step 1. (4) Pause for 42 s. (5) Repeat step 1. (6) Repeat steps 2–5 for 35 times.

To measure Golgi export rate of the protein of interest, the mean intensity of the region left by the photobleaching mask (Golgi-including region), $I(t)$, was measured over time and normalized to the initial intensity, $I_0 = I(t = 0)$, using ImageJ and plotted using Prism 9.1.2 (GraphPad). Data was finally fitted to a one-phase decay curve fixing the "plateau" to 0, that is $I(t)/I_0 = exp(-t/\tau)$, from where the half-life, $t_{1/2} = ln(2)\,\tau$, is extracted, and used to compare the Golgi residence time among different proteins.

**STORM imaging and data analysis**

For STORM imaging, HeLa cells were cultured on 8-chambered glass bottom dishes (Thermoscientific) at 37 °C with 5% $CO_2$. Plasmids containing the sequence of the gene of interest were transfected and 24 hours after, cells were fixed with 4% paraformaldehyde in PBS at room temperature for 15 minutes. After fixation, cells were washed, permeabilized with 0.1% Triton X-100 (Fisher Scientific) (v/v) in PBS for 10 minutes, washed again, and blocked in 3% BSA (Sigma Aldrich) (w/v) in PBS for 60 minutes. Then, cells were labeled with primary antibodies, as detailed in the "Immunofluorescence microscopy" section. Donkey-anti-rabbit conjugated with AF405/AF647 (3:1) and donkey-anti-mouse conjugated with Cy3/AF647 (7:1) were used as secondary antibodies at 2 µg/mL final concentration.

STORM was performed in an imaging buffer containing 10 mM Cysteamine MEA (SigmaAldrich), 0.5 mg/mL glucose oxidase (Sigma Aldrich), 40 µg/ml catalase (Sigma-Aldrich), and 6.25% glucose (Sigma Aldrich) in PBS [92]. Two-colour images were acquired on a commercial microscope system (Nikon Eclipse Ti N-STORM system), from Nikon Instruments, equipped with a 100x oil objective with NA 1.49 using oblique illumination. The detector was an ANDOR technology EMCCD iXon 897 camera, with a 256x256 pixel ROI and a pixel size of 160 nm. Fluorophore excitation was done using an Agilent technologies laser box with laser lines 405 nm, 561 nm, and 647 nm. NIS software (Nikon) was used for acquiring the data. In a pre-acquisition step the sample was irradiated with the 647 nm laser at 70% (~107 mW) power to bring a large majority of the dyes into a dark (off) state. STORM acquisition was then performed sequentially using 20 ms frames by maintaining the 647 nm laser at a constant power and using low power activator (405 nm or 561 nm) excitation (gradually increasing during acquisition from 0.5% to 100%). The acquisitions were stopped after ~70,000 frames.

STORM image reconstruction was performed in Insight3 software [93]. The generated images were also corrected for cross-talked from images obtained from samples only labelled with 1 pair of antibodies. For the image reconstruction, a list containing the localization data for each channel were obtained. The degree of colocalization between both lists of localization was measured within a Golgi- containing region of interest (ROI) using the Coloc-Tesseler software [94]. First, the software partition the image area into regions per localization where any given point within that region will be closer to that localization than to any other (Voronoi tessellation). Then, a first-rank density value, obtained from the area of the neighbour Voronoi areas, is assigned for each localization. Subsequently, these first-rank densities are represented in a logarithmic scaled scatterplot for each channel, always keeping channel A in x-axis and channel B in y-axis. The values in the scatterplot for channel A ($x^A$, $y^A$) correspond to the first-

rank density of a localization in channel A ($x^A$) against the first-rank density of the localization of channel B in whose Voronoi area the point in channel A landed ($y^A$). Vice versa for the scatterplot associated to channel B.

Finally, the Spearman's rank correlation coefficients are quantified as a measure of the trength and direction of the ranked variables plotted in each scatterplot. The Spearman's rank correlation coefficient is defined as $S^A = 1 - \frac{6\sum_i \left(r(x_i^A) - r(y_i^A)\right)^2}{n_A({n_A}^2 - 1)}$, and $S^B = 1 - \frac{6\sum_i \left(r(x_i^B) - r(y_i^B)\right)^2}{n_B({n_B}^2 - 1)}$, where $r(x_i^A)$ and $r(x_i^B)$ are the ranks of the first-rank density for channel A in the scatterplots A and B respectively; $r(y_i^A)$ and $r(y_i^B)$ are the ranks of the first-rank density of the channel B for the scatterplots A and B respectively; and $n_A$ and $n_B$ are the average number of neighbours per channel. As the Pearson's correlation coefficient, the Spearman's rank correlation coefficient varies from 1 (perfect localization) to -1 (perfect antilocalization) and 0 representing a random distribution of localizations.

**Protein deglycosylation**

Cells were detached from the surface of a well from a 6-well plate with Trypsin-EDTA (0.5%) (Gibco) for 5 min at 37ºC and 5% $CO_2$ and collected in a 1.5 mL tube. Upon trypsin removal by sample centrifugation, cells were lysed on ice with ice-cold 100 µL 0.5% Triton X-100 (Sigma-Aldrich) in PBS and sample was centrifuged at maximum speed for 20 min at 4ºC. 18 µL of sample lysate + 2 µL Denaturalization Buffer (New England Biolabs (NEB)) were incubated at 95ºC for 10 min. Then, each sample was completed with 4 µL Glycobuffer 1 (NEB), 4 µL NP-40 (NEB) and 8 µL $H_2O$. The reaction was then divided in 2 tubes (18 µL each) and 2 µL of Neuraminidase (NEB) or $H_2O$ was added. Samples were then incubated for 4 h at 37ºC and the reaction was stopped adding 4 µL Laemmli SDS sample buffer (6x) and incubated for 10 min at 95ºC. The samples were subjected to SDS-PAGE and Western blotted with anti-GFP (Santa Cruz) antibody.

**Immunoprecipitation**

HeLa cells were lysed with lysis buffer (0.5% Triton X-100 in PBS) containing protease inhibitors (Roche) for 15 min on ice, after which the samples were centrifuged at 16.000×g for 10 min at 4ºC. The resulting supernatants were incubated for 16 h while rotating at 4ºC with 8 µg/ml anti-GFP antibody (Roche). Protein A/G PLUS-Agarose (Santa Cruz) was then added to the samples and incubated with rotation for 2 h at 4ºC. Immunoprecipitated fractions were washed two times with lysis buffer and two more times with PBS, and heated to 95ºC for 5 min

with 1x Laemmli SDS sample buffer. The samples were subjected to SDS-PAGE and Western blotting with anti-GFP (Santa Cruz) and anti-RFP (Abcam) antibodies.

**Secretion assay**

The growth media of HeLa WT and HeLa TGN46 KO cells seeded on a well of 6-wells plate -and transfected with PAUF-Myc-His 48 h previous to the experiment performance- was exchanged by pre-warmed (37ºC) DMEM containing 1% penicillin/streptomycin and 2 mM L-Glutamine. Cells were then incubated for 4 h in an incubator at 37ºC and 5% $CO_2$ to collect secreted PAUF-Myc-His protein. Then, media was collected in a 1.5 mL tube and centrifuged to avoid floating dead cells that may interfere. Protease inhibitor was added to sample and sample was concentrated down to 150 µL using Amicon Ultra-0.5 10 kDa Centrifugal Filter Units (Merck). On the other hand, cells were lydes on ice with 150 uL of ice-cold lysis buffer (1% SDS Tris-HCl pH 7.4). Samples were collected in a 1.5 mL tube using a scraper and centrifuged at maximum speed for 20 min at 4ºC to remove cell pellet. Finally, 6x Laemmli SDS sample buffer was added to both, supernatant and cell samples, and incubated for 10 min at 95ºC. The samples were subjected to SDS-PAGE and Western blotting with anti-Myc (X) and anti-TGN46 (AbD Serotec) antibodies. When cells were treated with BFA, the compound was added to the cells to a final concentration of 5 µg/mL 15 min before media was exchanged by FBS-deprived media and also to the collection media for the 4 h incubation time of the secretion experiment.

**Protein production**

E. coli BL21 (DE3) cells transformed with pETM14-6his-mGFP -TGN46lum were grown at 37 °C to a density of OD600 0.6 in 2xYT medium containing Kanamycin (50 mg/l) with shaking. Isopropyl-β-D-thiogalactoside (IPTG) was added to induce protein expression at a final concentration of 0.2 mM, and the temperature was lowered to 18 °C. Cells were harvested after 16 h by centrifugation and resuspended in TRIS buffer supplemented with 300 mM NaCl, protease inhibitors (Roche), and lysed by French press cell disruptor. Lysate was clarified by centrifugation. The supernatant was loaded onto HisTrap HP 5 ml columns (Cytiva), washed and eluted by a linear gradient of 0–500 mM imidazole. The fractions containing the POI were pooled, concentrated using Amicon Ultra-15 30 kDa MWCO centrifugal filter unit (EMD Millipore), diluted in a TRIS buffer with 50ml NaCl and loaded onto a Hitrap Q 5ml column (Cytiva) washed and eluted by a linear gradient of 50–700 mM NaCl. The fractions containing the protein were collected, dialyzed again the storage buffer (20 mM TRIS pH7.4, 100 mM

NaCl and 10% glycerol), concentrated, and stored at −80 °C after flash freezing by liquid nitrogen.

### *In vitro* characterization of LLPS

The protein samples were dialyzed against 20 mM Tris-HCl and 1 mM TCEP at pH 7.5 and concentrated to approximately 150 μM. All samples were prepared on ice as follows. First, a buffer stock solution consisting of 20 mM Tris-HCl and 1mM TCEP was pH adjusted to 7.5 and filtered using 0.22 μm sterile filters (Buffer Stock). A 5 M NaCl solution in the same buffer was also pH adjusted to 7.5 and filtered (Salt Stock). Then, the protein samples were centrifuged for 5 minutes at 15,000 rpm at 5 ºC. The supernatant (Protein Stock) was transferred to a new Eppendorf tube and the protein concentration was determined by its absorbance at 280 nm. A 64% (w/v) Ficoll 70 in water solution was prepared (Ficoll Stock). The final samples were prepared by mixing the right amounts of Buffer Stock, Protein Stock, Salt Stock and Ficoll Stock to reach the desired final protein, NaCl and Ficoll concentrations.

For microscopy experiments, 1.5 μl of sample was deposited in a sealed chamber comprising a slide and a coverslip sandwiching double sided tape (3M 300 LSE high-temperature double-sided tape of 0.17 mm thickness). The used coverslips were previously coated with PEG-silane following the published protocol in Alberti et al [95]. Fluorescence microscopy images and FRAP experiments were recorded using a Zeiss LSM780 confocal microscope system with a Plan ApoChromat 63x 1.4 oil objective. For the FRAP experiment within a single droplet, 20 droplets of similar size were selected and the bleached region was 30% of their diameter. The intensity values were monitored for ROI1 (bleached area), ROI2 (entire droplet) and ROI3 (background signal), and the data was fitted using the EasyFrap software [96] to extract the kinetic parameters.

For the turbidity assay, the absorbance of the samples was measured at 350 nm at the indicated temperatures using 1 cm pathlength cuvettes and a Cary100 ultraviolet–visible spectrophotometer equipped with a multicell thermoelectric temperature controller.

### Statistics

Statistical significance was tested using One-Way ANOVA using GraphPad Prism 9.1.2, unless otherwise stated in the figure legend. Different data sets were considered to be statistically significant when the p-value was <0.05 (*); p-value<0.01 (**); p-value<0.001 (***); p-value<0.0001 (****).

## REFERENCES

1. Stalder, D. & Gershlick, D. C. Direct trafficking pathways from the Golgi apparatus to the plasma membrane. *Semin. Cell Dev. Biol.* **107**, 112–125 (2020).

2. Wakana, Y. & Campelo, F. The PKD-Dependent Biogenesis of TGN-to-Plasma Membrane Transport Carriers. *Cells 2021, Vol. 10, Page 1618* **10**, 1618 (2021).

3. Spang, A. The Road not Taken: Less Traveled Roads from the TGN to the Plasma Membrane. *Membranes (Basel).* **5**, 84–98 (2015).

4. von Blume, J. & Hausser, A. Lipid-dependent coupling of secretory cargo sorting and trafficking at the trans-Golgi network. *FEBS Lett.* **593**, 2412–2427 (2019).

5. Di Martino, R., Sticco, L. & Luini, A. Regulation of cargo export and sorting at the trans-Golgi network. *FEBS Lett.* **593**, 2306–2318 (2019).

6. Zappa, F., Failli, M. & De Matteis, M. A. The Golgi complex in disease and therapy. *Current Opinion in Cell Biology* **50**, 102–116 (2018).

7. Guo, Y., Sirkis, D. W. & Schekman, R. Protein sorting at the trans-Golgi network. *Annu. Rev. Cell Dev. Biol.* **30**, 169–206 (2014).

8. Boncompain, G. & Weigel, A. V. Transport and sorting in the Golgi complex: multiple mechanisms sort diverse cargo. *Current Opinion in Cell Biology* **50**, 94–101 (2018).

9. Ford, C., Parchure, A., von Blume, J. & Burd, C. G. Cargo sorting at the trans-Golgi network at a glance. *J. Cell Sci.* **134**, (2021).

10. Ramazanov, B. R., Tran, M. L. & von Blume, J. Sending out molecules from the TGN. *Current Opinion in Cell Biology* **71**, 55–62 (2021).

11. Kienzle, C. & von Blume, J. Secretory cargo sorting at the trans-Golgi network. *Trends in Cell Biology* **24**, 584–593 (2014).

12. Braulke, T. & Bonifacino, J. S. Sorting of lysosomal proteins. *Biochimica et Biophysica Acta - Molecular Cell Research* (2009). doi:10.1016/j.bbamcr.2008.10.016

13. Von Blume, J. *et al.* Actin remodeling by ADF/cofilin is required for cargo sorting at the trans-Golgi network. *J Cell Biol* **187**, 1055–1069 (2009).

14. Curwin, A. J., von Blume, J. & Malhotra, V. Cofilin-mediated sorting and export of specific cargo from the Golgi apparatus in yeast. *Molecular Biology of the Cell* **23**, 2327–2338 (2012).

15. von Blume, J. *et al.* ADF/cofilin regulates secretory cargo sorting at the TGN via the Ca2+ ATPase SPCA1. *Dev. Cell* **20**, 652–662 (2011).

16. Kienzle, C. *et al.* Cofilin recruits F-actin to SPCA1 and promotes Ca 2+ -mediated secretory cargo sorting. **206**, (2014).

17. Crevenna, A. H. *et al.* Secretory cargo sorting by Ca2+-dependent Cab45 oligomerization at the trans-Golgi network. *J. Cell Biol.* **213**, 305–314 (2016).

18. Blume, J. Von *et al.* Cab45 is required for Ca2+;-dependent secretory cargo sorting at the trans-Golgi network. *J. Cell Biol.* **199**, 1057–1066 (2012).

19. Deng, Y., Rivera-Molina, F. E., Toomre, D. K. & Burd, C. G. Sphingomyelin is sorted at the trans Golgi network into a distinct class of secretory vesicle. *Proc. Natl. Acad. Sci. U. S. A.* **113**, 6677–6682 (2016).

20. Deng, Y. *et al.* Activity of the SPCA1 Calcium Pump Couples Sphingomyelin Synthesis to Sorting of Secretory Proteins in the Trans-Golgi Network. *Dev. Cell* **47**, 464-478.e8 (2018).

21. Ponnambalam, S. *et al.* Primate homologues of rat TGN38: Primary structure, expression and functional implications. *J. Cell Sci.* **109**, 675–685 (1996).

22. Stanley, K. K. & Howell, K. E. TGN38/41: a molecule on the move. *Trends Cell Biol.* **3**, 252–255 (1993).

23. Jones, S. M., Crosby, J. R., Salamero, J. & Howell, K. E. A cytosolic complex of p62 and rab6 associates with TGN38/41 and is involved in budding of exocytic vesicles from the trans-Golgi network. *J. Cell Biol.* **122**, 775–788 (1993).

24. Wang, J., Ladinsky, M. S. & Howell, K. E. Molecules and vesicle coats involved in the budding of exocytotic vesicles from the trans-Golgi network. *Cold Spring Harb. Symp. Quant. Biol.* **60**, 139–146 (1995).

25. Banting, G. & Ponnambalam, S. TGN38 and its orthologues: roles in post-TGN vesicle formation and maintenance of TGN morphology. *Biochim Biophys Acta* **1355**, 209–217 (1997).

26. McNamara, J. O., Grigston, J. C., VanDongen, H. M. A. & VanDongen, A. M. J. Rapid dendritic transport of TGN38, a putative cargo receptor. *Mol. Brain Res.* **127**, 68–78 (2004).

27. Wang, J. & Howell, K. E. The luminal domain of TGN38 interacts with integrin β1 and is involved in its trafficking. *Traffic* **1**, 713–723 (2000).

28. Luzio, J. P. *et al.* Identification, sequencing and expression of an integral membrane protein of the trans-Golgi network (TGN38). *Biochem. J.* **270**, 97–102 (1990).

29. Bos, K., Wraight, C. & Stanley, K. K. TGN38 is maintained in the trans-Golgi network by a tyrosine-containing motif in the cytoplasmic domain. *EMBO J.* **12**, 2219–2228 (1993).

30. Rajasekaran, A. K. *et al.* TGN38 recycles basolaterally in polarized Madin-Darby canine kidney cells. *Mol. Biol. Cell* **5**, 1093–1103 (1994).

31. Mallet, W. G. & Maxfield, F. R. Chimeric forms of furin and TGN38 are transported from the plasma membrane to the trans-Golgi network via distinct endosomal pathways. *J. Cell Biol.* **146**, 345–359 (1999).

32. Humphrey, J. S., Peters, P. J., Yuan, L. C. & Bonifacino, J. S. Localization of TGN38 to the trans-Golgi network: involvement of a cytoplasmic tyrosine-containing sequence. *J. Cell Biol.* **120**, 1123–1135 (1993).

33. Wakana, Y. *et al.* A new class of carriers that transport selective cargo from the trans Golgi network to the cell surface. *EMBO J.* **31**, 3976–3990 (2012).

34. Wakana, Y. *et al.* Kinesin-5/Eg5 is important for transport of CARTS from the trans-Golgi network to the cell surface. *J. Cell Biol.* **202**, 241–250 (2013).

35. Lujan, P., Angulo-Capel, J., Chabanon, M. & Campelo, F. Interorganelle communication and membrane shaping in the early secretory pathway. *Current Opinion in Cell Biology* **71**, 95–102 (2021).

36. Zhang, J. *et al.* SARS-CoV-2 triggers Golgi fragmentation via down-regulation of GRASP55 to facilitate viral trafficking. *bioRxiv* 2022.03.04.483074 (2022). doi:10.1101/2022.03.04.483074

37. Hirschberg, K. *et al.* Kinetic Analysis of Secretory Protein Traffic and Characterization of Golgi to Plasma Membrane Transport Intermediates in Living Cells. *J. Cell Biol.* **143**, 1485 (1998).

38. Patterson, G. H. *et al.* Transport through the Golgi apparatus by rapid partitioning within a two-phase membrane system. *Cell* **133**, 1055–1067 (2008).

39. Malhotra, V. & Campelo, F. PKD regulates membrane fission to generate TGN to cell surface transport carriers. *Cold Spring Harb. Perspect. Biol.* **3**, 1–9 (2011).

40. Liljedahl, M. *et al.* Protein Kinase D regulates the fission of cell surface destined transport carriers from the trans-Golgi network. *Cell* **104**, 409–420 (2001).

41. Welch, L. G. & Munro, S. A tale of short tails, through thick and thin: investigating the sorting mechanisms of Golgi enzymes. *FEBS Lett.* **593**, 2452–2465 (2019).

42. Lujan, P. & Campelo, F. Should I stay or should I go? Golgi membrane spatial organization for protein sorting and retention. *Arch. Biochem. Biophys.* **707**, 108921 (2021).

43. Ohno, H., Fournier, M. C., Poy, G. & Bonifacino, J. S. Structural determinants of interaction of tyrosine-based sorting signals with the adaptor medium chains. *J. Biol. Chem.* (1996). doi:10.1074/jbc.271.46.29009

44. Banting, G., Maile, R. & Roquemore, E. P. The steady state distribution of humTGN46 is not significantly altered in cells defective in clathrin-mediated endocytosis. *J. Cell Sci.* **111**, 3451–3458 (1998).

45. Dunn, K. W., Kamocka, M. M. & McDonald, J. H. A practical guide to evaluating colocalization in biological microscopy. *Am. J. Physiol. - Cell Physiol.* **300**, C723 (2011).

46. Munro, S. Sequences within and adjacent to the transmembrane segment of alpha-2,6-sialyltransferase specify Golgi retention. *EMBO J.* **10**, 3577–3588 (1991).

47. Sharpe, H. J., Stevens, T. J. & Munro, S. A Comprehensive Comparison of Transmembrane Domains Reveals Organelle-Specific Properties. *Cell* **142**, 158–169 (2010).

48. Munro, S. An investigation of the role of transmembrane domains in Golgi protein retention. *EMBO J* **14**, 4695–4704 (1995).

49. Mitra, K., Ubarretxena-Belandia, I., Taguchi, T., Warren, G. & Engelman, D. M. Modulation of the bilayer thickness of exocytic pathway membranes by membrane proteins rather than cholesterol. *Proc. Natl. Acad. Sci. U. S. A.* **101**, 4083–4088 (2004).

50. Quiroga, R., Trenchi, A., Montoro, A. G., Taubas, J. V. & Maccioni, H. J. F. Short transmembrane domains with high-volume exoplasmic halves determine retention of type II membrane proteins in the golgi complex. *J. Cell Sci.* **126**, 5344–5349 (2013).

51. Cosson, P., Perrin, J. & Bonifacino, J. S. Anchors aweigh: protein localization and transport mediated by transmembrane domains. *Trends Cell Biol* **23**, 511–517 (2013).

52. Duran, J. M. J. M. *et al.* Sphingomyelin organization is required for vesicle biogenesis at the Golgi complex. *EMBO J.* **31**, 4535–4546 (2012).

53. van Galen, J. *et al.* Sphingomyelin homeostasis is required to form functional enzymatic domains at the trans-Golgi network. *J. Cell Biol.* **206**, 609–618 (2014).

54. Campelo, F. *et al.* Sphingomyelin metabolism controls the shape and function of the golgi cisternae. *Elife* **6**, (2017).

55. Capasso, S. *et al.* Sphingolipid metabolic flow controls phosphoinositide turnover at the trans -Golgi network . *EMBO J.* **36**, 1736–1754 (2017).

56. Banfield, D. K. Mechanisms of protein retention in the Golgi. *Cold Spring Harb. Perspect. Biol.* **3**, 1–14 (2011).

57. Banani, S. F., Lee, H. O., Hyman, A. A. & Rosen, M. K. Biomolecular condensates: organizers of cellular biochemistry. *Nat. Rev. Mol. Cell Biol. 2017 185* **18**, 285–298 (2017).

58. Garcia-Cabau, C. & Salvatella, X. Regulation of biomolecular condensate dynamics by signaling. *Curr. Opin. Cell Biol.* **69**, 111–119 (2021).

59. Shin, Y. & Brangwynne, C. P. Liquid phase condensation in cell physiology and disease. *Science (80-. ).* **357**, (2017).

60. Hyman, A. A., Weber, C. A. & Jülicher, F. Liquid-Liquid Phase Separation in Biology. *http://dx.doi.org/10.1146/annurev-cellbio-100913-013325* **30**, 39–58 (2014).

61. Brangwynne, C. P. *et al.* Germline P granules are liquid droplets that localize by controlled dissolution/condensation. *Science (80-. ).* **324**, 1729–1732 (2009).

62. Case, L. B., Ditlev, J. A. & Rosen, M. K. Regulation of Transmembrane Signaling by Phase Separation. *https://doi.org/10.1146/annurev-biophys-052118-115534* **48**, 465–494 (2019).

63. Lee, S. S. & Banting, G. Characterisation of the lumenal domain of TGN38 and effects of elevated expression of TGN38 on glycoprotein secretion. *Eur. J. Cell Biol.* **81**, 609–621 (2002).

64. Reaves, B., Horn, M. & Banting, G. TGN38/41 recycles between the cell surface and the TGN: brefeldin A affects its rate of return to the TGN. *Mol. Biol. Cell* **4**, 93–105 (1993).

65. Huet-Calderwood, C. *et al.* Novel ecto-tagged integrins reveal their trafficking in live cells. *Nat. Commun.* **8**, 1–13 (2017).

66. Yeaman, C. *et al.* Protein kinase D regulates basolateral membrane protein exit from

trans-Golgi network. *Nat. Cell Biol.* **6**, 106–112 (2004).

67. Lippincott-Schwartz, J. & Phair, R. D. Lipids and cholesterol as regulators of traffic in the endomembrane system. *Annual Review of Biophysics* **39**, 559–578 (2010).

68. van Meer, G., Voelker, D. R. & Feigenson, G. W. Membrane lipids: where they are and how they behave. *Nat. Rev. Mol. Cell Biol.* **9**, 112–124 (2008).

69. Bretscher, M. S. & Munro, S. Cholesterol and the Golgi apparatus. *Science (80-. ).* **261**, 1280–1281 (1993).

70. Milovanovic, D. *et al.* Hydrophobic mismatch sorts SNARE proteins into distinct membrane domains. *Nat. Commun.* **6**, 5984 (2015).

71. Diaz-Rohrer, B. B., Levental, K. R., Simons, K. & Levental, I. Membrane raft association is a determinant of plasma membrane localization. *Proc. Natl. Acad. Sci. U. S. A.* **111**, 8500–8505 (2014).

72. Lorent, J. H. *et al.* Structural determinants and functional consequences of protein affinity for membrane rafts. *Nat. Commun.* (2017). doi:10.1038/s41467-017-01328-3

73. Dmitrieff, S., Rao, M. & Sens, P. No Title. *Proc. Natl. Acad. Sci. U. S. A.* **110**, 15692–7 (2013).

74. Tu, L., Tai, W. C. S., Chen, L. & Banfield, D. K. Signal-mediated dynamic retention of glycosyltransferases in the Golgi. *Science (80-. ).* (2008). doi:10.1126/science.1159411

75. Wood, C. S. *et al.* PtdIns4P recognition by Vps74/GOLPH3 links PtdIns 4-kinase signaling to retrograde Golgi trafficking. *J. Cell Biol.* (2009). doi:10.1083/jcb.200909063

76. Welch, L. G., Peak-Chew, S. Y., Begum, F., Stevens, T. J. & Munro, S. Golph3 and golph3l are broad-spectrum copi adaptors for sorting into intra-golgi transport vesicles. *J. Cell Biol.* **220**, (2021).

77. Wakana, Y. *et al.* The ER cholesterol sensor SCAP promotes CARTS biogenesis at ER-Golgi membrane contact sites. *J. Cell Biol.* **220**, (2021).

78. Wakana, Y. *et al.* CARTS biogenesis requires VAP–lipid transfer protein complexes functioning at the endoplasmic reticulum–Golgi interface. *Mol. Biol. Cell* **26**, 4686–4699 (2015).

79. Luini, A. & Parashuraman, S. Signaling at the Golgi: Sensing and controlling the

membrane fluxes. *Current Opinion in Cell Biology* **39**, 37–42 (2016).

80. Cancino, J., Jung, J. E. & Luini, A. Regulation of Golgi signaling and trafficking by the KDEL receptor. *Histochemistry and Cell Biology* **140**, 395–405 (2013).

81. Kulak, N. A., Pichler, G., Paron, I., Nagaraj, N. & Mann, M. Minimal, encapsulated proteomic-sample processing applied to copy-number estimation in eukaryotic cells. *Nat. Methods 2014 113* **11**, 319–324 (2014).

82. Sengupta, D. & Linstedt, A. D. Control of organelle size: the Golgi complex. *Annu. Rev. Cell Dev. Biol.* **27**, 57–77 (2011).

83. Parchure, A. *et al.* Liquid-liquid phase separation facilitates the biogenesis of secretory storage granules. *bioRxiv* 2021.12.22.472607 (2021). doi:10.1101/2021.12.22.472607

84. Romero, Obradovic & Dunker. Sequence Data Analysis for Long Disordered Regions Prediction in the Calcineurin Family. *Genome Inform. Ser. Workshop Genome Inform.* **8**, 110–124 (1997).

85. Li, Romero, Rani, Dunker & Obradovic. Predicting Protein Disorder for N-, C-, and Internal Regions. *Genome Inform. Ser. Workshop Genome Inform.* **10**, 30–40 (1999).

86. Sickmeier, M. *et al.* DisProt: the Database of Disordered Proteins. *Nucleic Acids Res.* **35**, (2007).

87. Vacic, V., Uversky, V. N., Dunker, A. K. & Lonardi, S. Composition Profiler: a tool for discovery and visualization of amino acid composition differences. *BMC Bioinformatics* **8**, (2007).

88. Borgman, K. J. E. *et al.* Membrane receptor MerTK is a newly identified transcriptional regulator that associates to chromatin as nanoclusters during human DC differentiation. *bioRxiv* 2020.04.16.044974 (2020). doi:10.1101/2020.04.16.044974

89. Gibson, D. G. *et al.* Enzymatic assembly of DNA molecules up to several hundred kilobases. *Nat Methods* **6**, 343–345 (2009).

90. Pecot, M. Y. & Malhotra, V. Golgi membranes remain segregated from the endoplasmic reticulum during mitosis in mammalian cells. *Cell* **116**, 99–107 (2004).

91. Bossard, C., Bresson, D., Polishchuk, R. S. & Malhotra, V. Dimeric PKD regulates membrane fission to form transport carriers at the TGN. *J. Cell Biol.* **179**, 1123–1131 (2007).

92. Gómez-García, P. A., Garbacik, E. T., Otterstrom, J. J., Garcia-Parajo, M. F. & Lakadamyali, M. Excitation-multiplexed multicolor superresolution imaging with fm-STORM and fm-DNA-PAINT. *Proc. Natl. Acad. Sci. U. S. A.* **115**, 12991–12996 (2018).

93. Huang, B., Wang, W., Bates, M. & Zhuang, X. Three-Dimensional Super-Resolution Reconstruction Microscopy. *Science (80-. ).* **319**, 810–813 (2008).

94. Levet, F. *et al.* A tessellation-based colocalization analysis approach for single-molecule localization microscopy. *Nat. Commun. 2019 101* **10**, 1–12 (2019).

95. Alberti, S. *et al.* A User's Guide for Phase Separation Assays with Purified Proteins. *J. Mol. Biol.* **430**, 4806–4820 (2018).

96. Rapsomaniki, M. A. *et al.* easyFRAP: an interactive, easy-to-use tool for qualitative and quantitative analysis of FRAP data. *Bioinformatics* **28**, 1800–1801 (2012).